UNIVERSITÀ POLITECNICA DELLE MARCHE
Faculty of Medicine and Surgery
Department of Biomedical Sciences and Public Health
PhD Course in Biomedical Sciences (XXXV cycle)

Structure elucidation of novel synthetic opioid metabolites: New biomarkers of exposure in clinical and forensic toxicology

Candidate:	**Tutor:**	**Supervisor:**
Dott. Pietro Brunetti	Prof. Francesco Paolo Busardò	Prof. Volker Auwärter

A.A. 2021-2022

Summary

1. Introduction

With "Spice" (advertised as a "legal alternative" to cannabis), the new psychoactive substances (NPS) began to appear on the market from around 2004 [1]. Offered as "legal highs", "research chemicals", bath salts and dietary supplements, these drugs spread on the Internet under the guise of legality [2]. In recent years, more and more NPS came onto the market causing numerous overdoses and repeated deaths [3].

According to the United Nation Office of Drugs and Crime (UNODC), NPS are new psychotropic or narcotic substances, in pure form or as a preparation, that are not included in the 1961 and 1971 United Nations Conventions on narcotic drugs and psychotropic substances, but which may pose a public health threat that is comparable to the compounds listed there [1,4]. The term “new” does not necessarily refers to new inventions but to substances that have recently become available on the market.

Large-scale production of NPS usually takes place in China or India from where they reach Europe and the US often as undeclared products of low value [5]. Consumers are not always aware that they are purchasing NPS or which NPS they are buying, resulting in an increasing number of adverse health events, including emergency room admissions and death investigations [2,6]. Like in a cat-and-mouse game, as soon as a substance is discovered on the market, investigated and controlled/banned, new substances appear [5]. In this scenario, the European Monitoring Center for Drugs and Drug Addiction (EMCDDA) plays a central role in drug surveillance. So far, approximately 880 NPS (as of the end of 2021) have been reported in the EU [7].

Owing their pharmacotoxicological profile, NPS can be divided in synthetic cannabinoid receptor agonists, dissociatives, hallucinogens, stimulants and depressants, including novel synthetic opioids (NSOs) and designer benzodiazepines [8]. NSOs in particular are of great concern due to the risk of respiratory depression [9].

1.1 Novel Synthetic Opioids

Since their introduction into the illegal drug market, NSOs have been misused in place of heroine, gaining popularity due to their cheaper cost and easiness to conceal and transport. NSOs are manufactured and sold as powders, liquids, tablets and capsules, or, more recently,

as liquids for e-cigarettes or in the form of infused papers [10,11]. It was postulated that NSOs mainly act as selective μ-opioid receptor (MOR) agonists, displaying various degrees of potency and efficacy, most of them being more potent than morphine, entailing a higher risk of overdose [12,13]. Adverse effects reported after NSO intake include nausea, hypothermia, sedation, drowsiness and respiratory depression [14]. So far, 73 compounds belonging to different classes of basic chemical structures were reported to the EMCDDA [12,15].

1.1.1 Fentanyls

Fentanyl is an analgesic synthetic opioid of the phenylpiperidine family. It was originally synthesized in Belgium by Paul Janssen in 1959 as a derivative of meperidine [9]. The potency of fentanyl is 50-100 times higher than that of morphine and 25-40 times higher than that of heroin, it has high lipophilicity and easily crosses the blood-brain barrier. Fentanyl analogs (FAs) are structurally and pharmacologically related to fentanyl with minor substitutions of the propionyl chain and/or the phenylethyl moiety [2].

Since 2012, FAs have ruled the illegal opioid market, contributing to the "opioid epidemic crisis" with more than 130,000 deaths in North America [16,17]. Meanwhile, in some parts of Europe, owing to a shortage in the availability of classical opioids, FAs have established themselves as the most trafficked NSOs [18,19].

β'-Phenylfentanyl also called 3-phenylpropanoylfentanyl, is a fentanyl analogue substituted with a phenyl ring at the terminal carbon of the propanamide chain It was first detected in Sweden and reported to the EMCDDA in May 2017 [20]. Recent β'-phenylfentanyl seizures in Canada and the USA reported to the UNODC early warning advisory indicated recent reemergence onto the illicit drug market [21].

1.1.2 Acylpiperazine opioids (APs)

In contrast to FAs, the chemical structure of APs is characterized by a piperazine core and a cinnamyl moiety instead of the piperidine and the phenethyl chain (Figure 1).

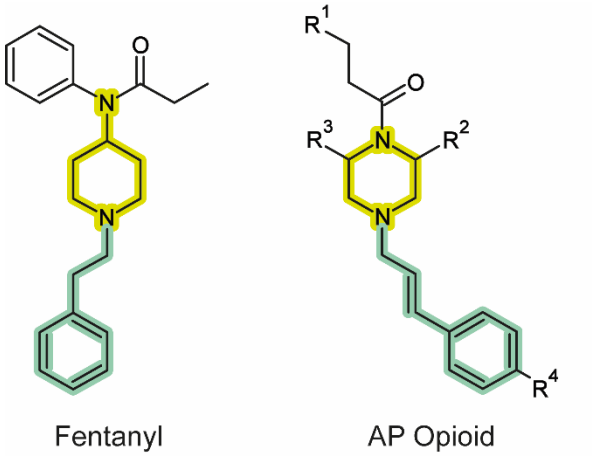

Figure 1. *Acylpiperazine opioids in comparison to fentanyl.*

The prototype of this structural class is AP-237, also known as bucinnazine. First synthesized in 1968, AP-237 was found to be a potent analgesic in animal models with better oral efficacy and less dependence liability than morphine [24-26]. In China, AP-237 is an approved drug used as a moderate intensity analgesic for patients suffering from migraine, traumatic pain, trigeminal neuralgia and cancer-related pain, but it has so far not been approved for medical use elsewhere [25,26].

In 2020, the 2,6-dimethyl propionyl analog of AP-237, namely AP-238 (IUPAC name: 1-{2,6-dimethyl-4-[(2E)-3-phenylprop-2-en-1-yl]piperazine-1-yl}propan-1-one), started to circulate via Internet shops and was involved in a case of fatal intoxication [27,28]. Despite the long (pre)clinical history of AP compounds, deeper knowledge concerning their pharmacological and toxicological properties is still lacking in the available literature. In 1968, Cigarella et al. synthesized a series of compounds structurally related to the analgetic 8-acyl-3,8-diazabicyclo[3.2.1]octanes, with AP-238 (compound VII in the reference) being about two times more potent than morphine with regard to analgesia and acute toxicity in rodents, whit a shorter duration of action [29]. More recently, Fogarty et al. characterized a wide panel of NSOs using an in vitro MOR activation assay. AP-238 resulted as the most potent drug in this subclass with an EC_{50} of 248 nM, 95% CI: 184-333 nM (hydromorphone: EC_{50} of 26.9 nM, 95% CI: 19.9-36.4 nM), but considerably less potent than fentanyl [13,30].

1.2 Analysis and screening methods

Rapid identification of NSOs can aids in the proper and effective treatment of overdoses and provides epidemiological data for their monitoring. In clinical and forensic toxicology, biological samples (e.g. blood, urine, hair, oral fluid) are screened and/or quantified to identify drug of abuse and their characteristic metabolites [2, 30]. NSOs present analytical challenges compared to classical opioids, on one hand, this group includes a large number of substances that is constantly growing, on the other hand, many toxicological and toxicokinetic properties, such as metabolization, are mostly unknown at the time of their occurrence [2]. Thus, the total number of NSOs and related intoxications are likely underestimated, in addition the low concentrations in biological matrices are challenging to detect, especially in cases of polydrug consumption. Therefore, the identification of specific metabolite biomarkers is often required to prove NSOs consumption.

In most cases, immunoassays for established drugs that are easy to perform do not detect NPS and their development is made more difficult by the constant change in the NPS market [1,31]. For these reasons, liquid-chromatography coupled with high-resolution mass spectrometry (LC-HRMS) is primarily used for the identification and structural elucidation of NPS and their metabolites due to its selectivity, sensitivity and flexibility [32,33].

1.3 Aims and Objectives

In this dissertation, the metabolism of two NSOs was investigated to propose suitable biomarkers of exposure in clinical and forensic toxicology. The first experiment was performed at the laboratory of forensic toxicology of the University of Ancona (Italy), here the β'-phenylfentanyl in vitro phase I and phase II metabolic pathway was studied using cryopreserved primary human hepatocytes. Incubates were analyzed by LC–HRMS and software-assisted data mining with a targeted/untargeted workflow for a comprehensive screening. A second set of experiments was conducted at the Institute of Forensic Medicine of the University of Freiburg (Germany). Here the phase I metabolism of AP-238 was investigated using in vitro incubations with pooled human liver microsomes (pHLMs) and real samples by means of LC–HRMS. Finally, the most reliable urinary markers were evaluated performing a controlled oral self-administration study.

2. In vitro metabolism of β'-phenylfentanyl

2.1 Material and methods

2.1.1 In silico metabolite prediction

β'-Phenylfentanyl putative metabolites were predicted using GLORYx freeware [34,35]. The metabolite list was generated using the 'phase I and phase II metabolism' option. Metabolites with a score higher than 20% were selected and reprocessed to simulate a second-step reaction. The score of the second-generation metabolites was multiplied to the score of the corresponding first-generation metabolite to provide an adjusted score; adjusted scores higher than 20% were considered.

2.1.2 Chemicals and reagents

β'-phenylfentanyl, 4-ANPP (Cayman chemical; Ann Harbor, MI, USA), and diclofenac (Sigma Aldrich; Milan, Italy) standards were dissolved in LC-MS grade methanol (Carlo Erba; Cornaredo, Italy) to 1-mg/mL stock solutions. The solutions were stored at –20 °C until analysis. Ten-donor-pooled cryopreserved human hepatocytes, thawing medium (TM), and 0.4% trypan blue were purchased from Lonza (Basel, Switzerland). L-Glutamine, HEPES (2-[4-(2-hydroxyethyl)-1-piperazinyl]ethanesulfonic acid), and Williams' Medium E were purchased from Sigma Aldrich. L-Glutamine and HEPES were dissolved in Williams' Medium E to 2 and 20 mmol/L, respectively, prior to analysis. The supplemented Williams' Medium E (sWME) was stored at 4°C until incubation. LC-MS grade acetonitrile (ACN), water, and formic acid were purchased from Carlo Erba. Mobile phase A (0.1% HCOOH in water) and mobile phase B (0.1% HCOOH in ACN) were freshly prepared prior to analysis.

2.1.3 Hepatocyte incubation

Incubations were conducted as previously described [33]. Hepatocytes were thawed at 37 °C and gently mixed in 50 mL TM at 37 °C in a 50-mL polypropylene conical tube. The tube was centrifuged at 100 g for 5 min and the pellet was washed with 50 mL sWME at

37 °C. After centrifugation at 100 g for 5 min, the cells were resuspended in 2 mL sWME. Hepatocyte viability was assessed with the trypan blue exclusion test, and sWME volume was adjusted to 2 x 106 viable cells/mL.

Incubations were prepared in sterile 24-well culture plates with 250 µL hepatocyte suspension at 2 x 106 viable cells/mL in sWME at 37 °C and 250 µL β'-phenylfentanyl at 20 µmol/L in sWME at 37 °C. The samples were placed in an incubator previously set at 37 °C (Argo Lab; Carpi, Italy) and metabolic reactions were stopped with 500 µL ice-cold acetonitrile after 0 h or 3 h. The samples were transferred into microtubes, centrifuged for 10 min, 15,000 g, at room temperature, and prepared for analysis.

Diclofenac was incubated under the same conditions, and 4'-hydroxydiclofenac and diclofenac acyl-β-D-glucuronide were monitored to ensure proper metabolic activity. In addition, negative controls i.e. hepatocytes in sWME without β'-phenylfentanyl and β'-phenylfentanyl in sWME without hepatocytes were prepared to assess spontaneous reactions.

2.1.4 Sample preparation

After sample centrifugation, 100 µL of supernatant was vortex mixed with 100 µL ACN and centrifuged for 10 min, 15,000 g, at room temperature. The supernatants were dried under nitrogen at 37 °C and the residues were reconstituted with 150 µL of A:B (8:2 v/v). After centrifugation for 10 min, 15,000 *g*, at room temperature, supernatants were transferred into LC autosampler vials with glass inserts.

2.1.5 Identification of tentative main metabolites with LC-HRMS-MS

LC-HRMS/MS analyses were performed on a DIONEX UltiMate 3000 liquid chromatographer coupled with a Q-Exactive quadrupole-Orbitrap hybrid HRMS equipped with a heated electrospray ionization (HESI) source (Thermo Scientific, Waltham, MA, USA).

The chromatographic separation was performed on a Kinetex® Biphenyl column (150 x 2.1 mm, 2.6 µm) from Phenomenex. Elution was achieved within 30 min with the

gradient started with 5% B held for 2 min; B was increased to 50% within 16 min then 95% within 2 min and held for 5 min before returning to initial conditions within 0.1 min; re-equilibration time was 4.9min. The flow rate was set to 0.4 mL/min. Autosampler and oven temperatures were 10 ± 1 and 37 ± 1 °C, respectively. The injection volume was 15 µL. Samples were injected twice, in positive and negative-ion modes.

The orbitrap was calibrated prior to analysis and a lock mass list was used for better accuracy (*m/z* 100.07570, 149.0233, and 391.2843 in positive-ion mode, *m/z* 96.9601 and 112.9856 in negative-ion mode [36]. HESI parameters were: sheath gas flow rate, 50 a.u.; auxiliary gas flow rate, 10 a.u.; spray voltage, ±3 kV (positive- and negative-ionization modes); capillary temperature, 300 °C; auxiliary gas temperature, 300 °C; S-lens radio frequency level, 50 a.u. and sweep gas flow rate, none. The mass spectrometer acquired data from 1 to 25 min of the LC gradient in full-scan HRMS (FullMS)/data dependent MS-MS ($ddMS^2$) mode.

Data were acquired with Thermo Scientific Xcalibur (v. 4.1.31.9). The FullMS acquisition range was *m/z* 80-770 with a resolution of 70,000 at full width at half maximum at *m/z* 200; automatic gain control (AGC) target was 2×105 and maximum injection time (IT) was 200 ms. Up to five $ddMS^2$ scans were triggered for each FullMS scan depending on a priority inclusion list of putative metabolites based on in silico predictions and the metabolic fate of β'-phenylfentanyl analogues [33,37] (Table 1); $ddMS^2$ isolation window was *m/z* 1.2 with a resolution of 17,500; normalized collision energy was 30, 35 and 50 a.u.; AGC target was 2×10^5 and maximum IT was 64 ms; intensity threshold for triggering MS^2 spectra was 6.5×10^2, with a dynamic exclusion of 2.0 s. LC-HRMS-MS raw data were processed with

Table 1. *Iinclusion list for the β'-phenylfentanyl MS^2 data depending acquisition*

Transformation	**Molecular formula**	**[M + H]+ (*m/z*)**	**[M – H]- (*m/z*)**
β'-phenylfentanyl	$C_{28}H_{32}N_2O$	413.2587	411.2442
-20C-22H-2N	$C_8H_{10}O$	123.0804	121.0659
-19C-21H-N	$C_9H_{11}NO$	150.0913	148.0768
-19C-22H-2N+O	$C_9H_{10}O_2$	151.0754	149.0608
-15C-13H-N	$C_{13}H_{19}NO$	206.1539	204.1394
-13C-17H-N	$C_{15}H_{15}NO$	226.1226	224.1081
-13C-17H-N+O	$C_{15}H_{15}NO_2$	242.1176	240.1030
-12C-15H-N+O	$C_{16}H_{17}NO_2$	256.1332	254.1187
-13C-17H-N+2O	$C_{15}H_{15}NO_3$	258.1125	256.0979
-13C-15H-N+2O	$C_{15}H_{17}NO_3$	260.1281	258.1136
-9C-8H-O	$C_{19}H_{24}N_2$	281.2012	279.1867
-9C-8H	$C_{19}H_{24}N_2O$	297.1961	295.1816
-8C-8H	$C_{20}H_{24}N_2O$	309.1961	307.1816
-8C-6H	$C_{20}H_{26}N_2O$	311.2118	309.1972
-9C-8H+O	$C_{19}H_{24}N_2O_2$	313.1911	311.1765
-9C-6H+O	$C_{19}H_{26}N_2O_2$	315.2067	313.1922
-13C-17H-N+4O+S	$C_{15}H_{15}NO_5S$	322.0744	320.0598
-8C-8H+O	$C_{20}H_{24}N_2O_2$	325.1911	323.1765
-7C-6H+O	$C_{21}H_{26}N_2O_2$	339.2067	337.1922
-8C-8H+2O	$C_{20}H_{24}N_2O_3$	341.1860	339.1714
-8C-6H+2O	$C_{20}H_{26}N_2O_3$	343.2016	341.1871
-9C-8H+3O+S	$C_{19}H_{24}N_2O_4S$	377.1530	375.1384
-8C-8H+4O+S	$C_{20}H_{24}N_2O_5S$	405.1479	403.1333
-2H	$C_{28}H_{30}N_2O$	411.2431	409.2285
-7C-9H-N+7O	$C_{21}H_{23}NO_8$	418.1496	416.1351
-2H+O	$C_{28}H_{30}N_2O_2$	427.2380	425.2235
+O	$C_{28}H_{32}N_2O_2$	429.2537	427.2391
+C+2H+O	$C_{29}H_{34}N_2O_2$	443.2693	441.2548
+2O	$C_{28}H_{32}N_2O_3$	445.2486	443.2340
+2H+2O	$C_{28}H_{34}N_2O_3$	447.2642	445.2497
+C+2H+2O	$C_{29}H_{34}N_2O_3$	459.2642	457.2497
-3C+6O	$C_{25}H_{32}N_2O_7$	473.2282	471.2137
-2C+7O	$C_{26}H_{32}N_2O_8$	501.2231	499.2086
4O+S	$C_{28}H_{32}N_2O_5S$	509.2105	507.1959
+5O+S	$C_{28}H_{32}N_2O_6S$	525.2054	523.1908
+6C+8H+7O	$C_{34}H_{40}N_2O_8$	605.2857	603.2712
+6C+8H+8O	$C_{34}H_{40}N_2O_9$	621.2807	619.2661
+7C+10H+8O	$C_{35}H_{42}N_2O_9$	635.2963	633.2818
10C+17H+3N+7O+S	$C_{38}H_{49}N_5O_8S$	736.3375	734.3229

2.1.6 Data pre-processing

The raw data from samples and controls were processed simultaneously. All spectra were selected, and the retention times of the relative chromatographic peaks were aligned between the files to facilitate comparison, following an adaptive curve model, with a maximum shift of 0.1 min and a mass tolerance of 5 ppm. A base peak chromatogram was generated in full-scan HRMS in positive- and negative-ion modes. Aligned spectra were then further processed using a targeted/untargeted approach (Figure 2) [33].

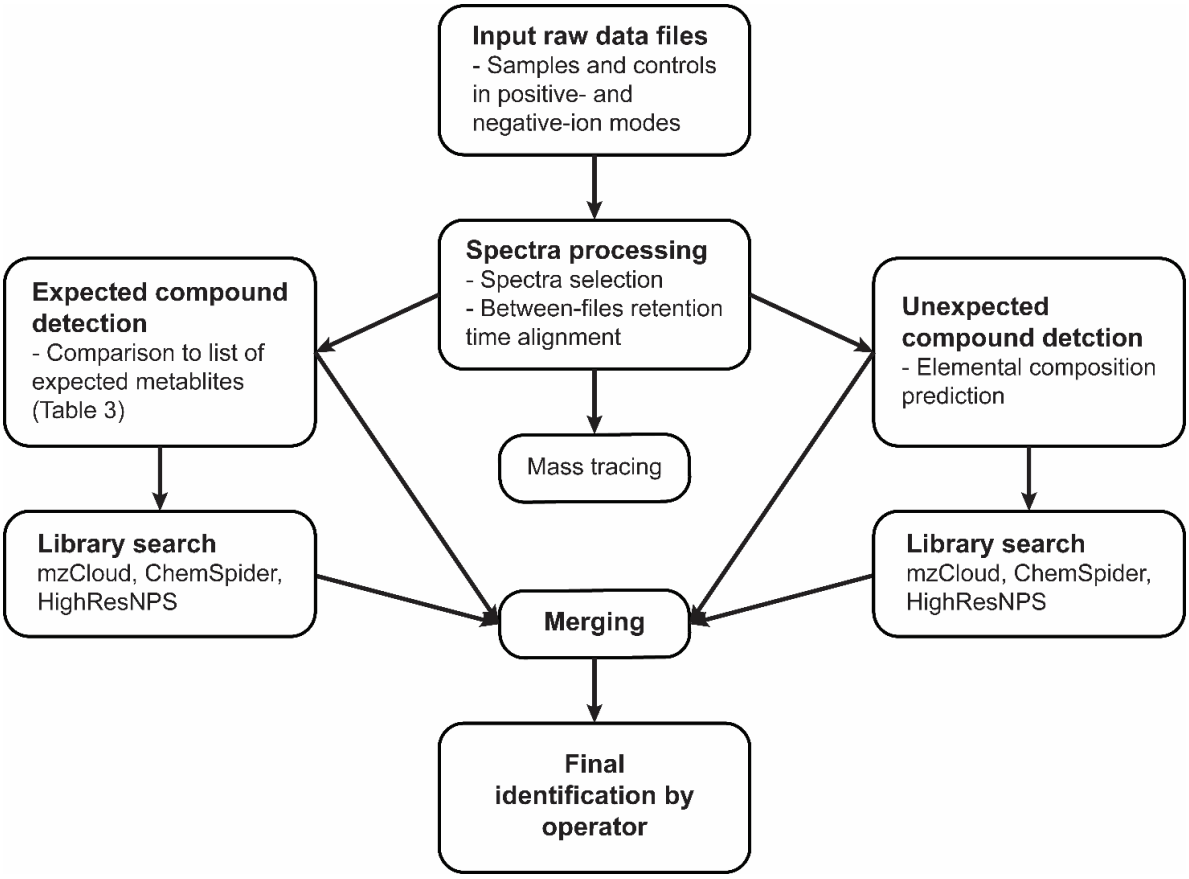

Figure. 2. *LC-HRMS/MS raw data processing workflow*

2.1.6.1 Untargeted data mining

Chromatographic peaks with an intensity higher than 10^6, a signal/noise ratio higher than 3, and a 30% intensity tolerance for isotopes were selected; peaks with fewer than 3 scans or larger than 0.5 min were excluded. When applicable, $[M+H]^+$, $[M+Na]^+$, $[M+K]^+$, $[M+NH_4]^+$, $[M+H-H_2O]^+$, $[M-H]^-$, $[M+Cl]^-$, and $[M+HCOOH]^-$ adducts were grouped (5-ppm mass tolerance) and $[M+H]^+$ adduct was used as base ion. Unknown compounds were grouped across the data files with a 5-ppm mass tolerance and a 0.1-min retention time tolerance, and their elemental composition was predicted within a C_7H_6 to $C_{36}H_{50}N_5O_{12}S_2$ range. $ddMS^2$ spectra and molecular formulas were compared to selected libraries: mzCloud™ (Drugs of Abuse/Illegal Drugs database), ChemSpider (Cayman Chemical and DrugBank databases), and HighResNPS. mzCloud™ is a database containing the mass spectra and product-ion spectra at different collision energies of approximately 20,000 compounds in the fields of life sciences, metabolomics, pharmaceutical research, toxicology, forensic investigations, environmental analysis, food control, and industrial applications [38]. ChemSpider is a database containing various information on more than 100 million chemicals from over 270 data sources [39]. HighResNPS is a crowd-sourced HRMS database containing the mass spectra of NPS with over 5200 entries, among which 2100 are unique [40]. The results from targeted and untargeted data mining approaches were merged, and the compounds detected in controls with a similar or higher intensity than those detected in phenylfentanyl incubations were filtered out. The results were finally screened by the operator for final identification and structural elucidation.

2.1.6.2 Targeted data mining

A list of theoretical metabolites was generated by combining probable phase I and phase II metabolic transformations, following the settings displayed in Table 3. Chromatographic peaks with an intensity higher than 5×10^3, a signal/noise ratio higher than 3, and a 30% intensity tolerance for isotopes were compared to the list of expected compounds with a 5-ppm mass tolerance. Compounds were grouped across the data files with a 0.1-min retention time tolerance and compared to mzCloud™, ChemSpider, and HighResNPS libraries.

2.2 Results and Discussion

β'-phenylfentanyl fragmentation pattern was consistent with the scientific literature (Figure 3). In positive-ionization mode, ion *m/z* 188.1434 was produced by the phenylethylpiperidine moiety of the molecule and was the fragment with the most intense signal; further fragmentation produced ions *m/z* 132.0807, 134.0964 and 146.0964. The second most intense fragment was *m/z* 105.0699, produced by the two phenethyl groups, which made the structure elucidation of several metabolites challenging. Ions *m/z* 281.2011 (4-ANPP) and 292.1695 were minor. β'-phenylfentanyl was not detected in negative-ionization mode.

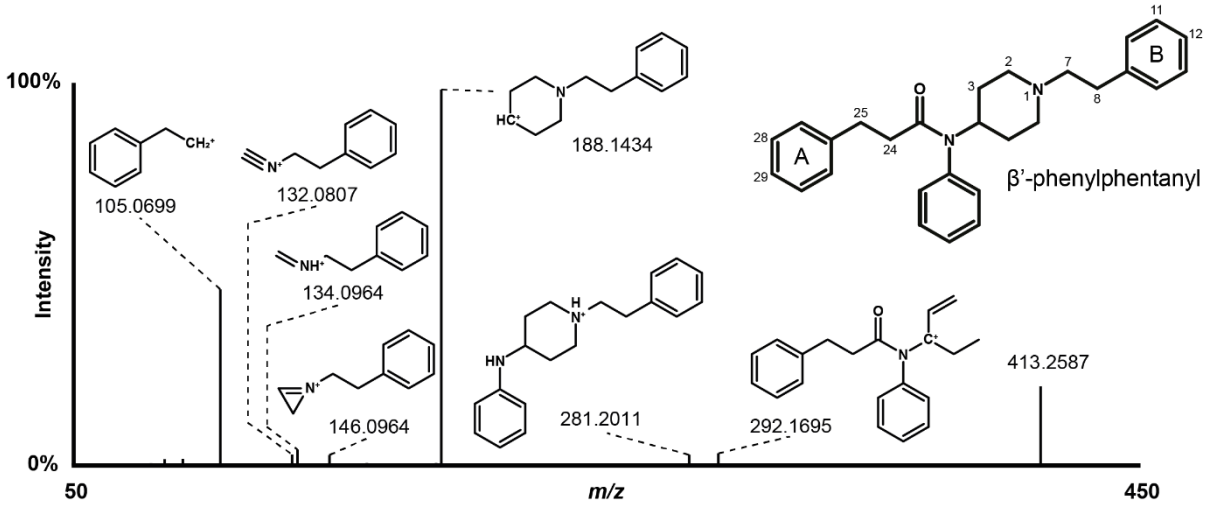

Figure 3. *β'-phenylfentanyl high-resolution tandem mass spectrometry spectrum and suggested fragmentation in positive-ionization mode.*

Raw LC–HRMS-MS data were automatically processed within 4 h 35 min to produce a list of 161 potential metabolites that were manually checked by the operators. β'-Phenylfentanyl LC–HRMS-MS peak area was 2.08×10^{10} in the 0h incubate with hepatocytes, which was approximately 15 times higher than that of the 3h incubate. Twenty-six metabolites were identified (20 phase I and 6 phase II metabolites) and were listed from M1 to M26 by ascending retention time (Figure 4,5; Table 2). Major phase I transformations included *N*-dealkylation at the piperidine ring to produce β'-phenylfentanyl and further metabolites (M2-M5, M7, M9-M13, M17, M19, M23 and M25), hydroxylation

(M9, M16, M18 and M22) and oxidation (M13, M20, M21, M24 and M26) at C25, and dihydrodiol formation at the phenyl ring of the phenylpropanamide moiety (M2, M6, M8 and M14); other transformations were *N*-dealkylation to 4-hydroxy-1-(2-phenylethyl)piperidine (M1), hydroxylation at the phenyl ring of the phenylpropanamide moiety (M3, M4, M7, M10–M12 and M15) and the *N*-phenethyl moiety (M8 and M20), hydroxylation (M19 and M20) and oxidation (M23, M25 and M26) at the piperidine ring. Phase II transformations were observed in minor metabolites: glucuronidation (M3–M5, M15 and M16) and methylation (M3 and M10) were detected. 4-ANPP was not detected in incubates.

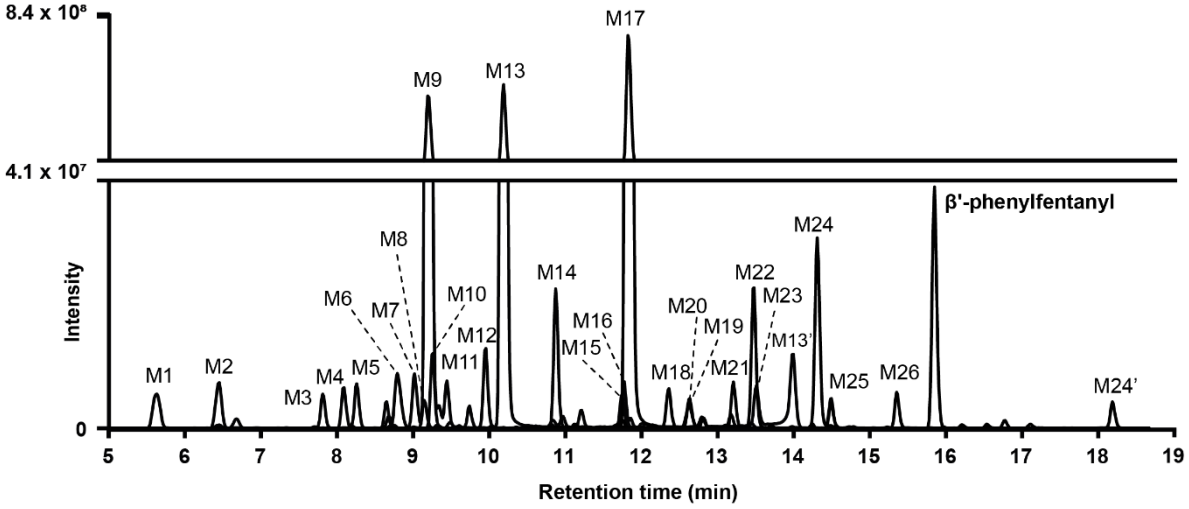

Figure 4. *Extracted-ion chromatogram of β'-phenylfentanyl and metabolites in positive-ionization mode obtained after 3h incubation with human hepatocytes. Mass tolerance, 5 ppm.*

Table 2. *Metabolic Transformation, Retention Time (RT), Accurate Mass of Molecular Ion (Hydrogen Adduct in Positive-Ionization Mode $[M+H]^+$), Elemental Composition, Deviation from Theoretical Accurate Mass, and Liquid Chromatography-High-Resolution Mass Spectrometry Peak Area of β'-Phenylfentanyl and Metabolites after 3-h Incubation with Human Hepatocytes*

ID	Transformation	RT (min)	$[M+H]^+$ (*m/z*)	Elemental composition	Mass error (ppm)	LC-HRMS peak area
M1	*N*-Dealkylation (amide)	5.63	206.1541	$C_{13}H_{19}NO$	0.56	4.49×10^7
M2	*N*-Dealkylation (piperidine) + Dihydrodiol formation (phenyl A)	6.45	343.0180	$C_{20}H_{26}N_2O_3$	0.38	5.23×10^7
M3	*N*-Dealkylation (piperidine) + Dihydroxylation (phenyl A) + *O*-Methylation + *O*-Glucuronidation	7.81	531.2342	$C_{27}H_{34}N_2O_9$	0.92	3.24×10^7
M4	*N*-Dealkylation (piperidine) + Hydroxylation (phenyl A) + *O*-Glucuronidation	8.09	501.2234	$C_{26}H_{32}N_2O_8$	0.29	4.03×10^7
M5	*N*-Dealkylation (piperidine) + Hydroxylation (piperidine) + *O*-Glucuronidation	8.26	501.2233	$C_{26}H_{32}N_2O_8$	0.32	4.30×10^7
M6	+4O+4H (phenylpropanamide)	8.79	481.2697	$C_{28}H_{36}N_2O_5$	0.04	7.45×10^7
M7	*N*-Dealkylation (piperidine) + Hydroxylation (phenyl A)	9.02	325.1911	$C_{20}H_{24}NO_7$	0.05	4.94×10^7
M8	Dihydrodiol formation (phenyl A) + Hydroxylation (phenyl B)	9.14	463.2591	$C_{28}H_{34}N_2O_4$	-0.09	2.73×10^7
M9	*N*-Dealkylation (piperidine) + Hydroxylation (ethyl of phenylpropanamide)	9.14	325.1910	$C_{20}H_{24}N_2O_2$	-0.15	2.07×10^9
M10	*N*-Dealkylation (piperidine) + Dihydroxylation (phenyl A) + Methylation	9.25	355.2016	$C_{21}H_{26}N_2O_3$	-0.05	6.23×10^7
M11	*N*-Dealkylation (piperidine) + Hydroxylation (phenyl A)	9.44	325.1911	$C_{20}H_{24}N_2O_2$	-0.15	4.25×10^7
M12	*N*-Dealkylation (piperidine) + Hydroxylation (phenyl A)	9.95	325.1911	$C_{20}H_{24}N_2O_3$	-0.13	7.02×10^7
M13	N-Dealkylation (piperidine) + Oxidation (ethyl of phenylpropanamide)	10.18	323.1754	$C_{20}H_{22}N_2O_2$	-0.17	2.34×10^9
M14	Dihydrodiol formation (phenyl A)	10.87	447.2644	$C_{28}H_{34}N_2O_3$	0.35	1.29×10^8
M15	Dihydroxylation (phenyl A) + *O*-Glucuronidation	11.74	621.2806	$C_{34}H_{40}N_2O_9$	-0.03	3.49×10^7
M16	Hydroxylation (ethyl of phenylpropanamide) + O-Glucuronidation	11.76	605.2859	$C_{34}H_{40}N_2O_8$	0.23	4.80×10^7
M17	*N*-Dealkylation (piperidine)	11.82	309.1960	$C_{20}H_{24}N_2O$	-0.50	3.91×10^9
M18	Hydroxylation (ethyl of phenylpropanamide) + Hydroxylation (piperidine)	12.35	445.2487	$C_{28}H_{32}N_2O_3$	0.27	4.09×10^7
M19	*N*-Dealkylation (piperidine) + Hydroxylation (piperidine)	12.62	325.1912	$C_{20}H_{24}N_2O_2$	0.34	2.66×10^7
M20	Oxidation (ethyl of phenylpropanamide) + Hydroxylation (phenyl B)	12.63	443.2331	$C_{28}H_{30}N_2O_3$	0.46	3.06×10^7
M21	Oxidation (ethyl of phenylpropanamide) + Hydroxylation (piperidine)	13.21	443.2331	$C_{28}H_{30}N_2O_4$	0.30	4.31×10^7
M22	Hydroxylation (ethyl of phenylpropanamide)	13.47	429.2537	$C_{28}H_{32}N_2O_2$	0.15	1.39×10^8

M23	*N*-Dealkylation (piperidine) + Oxidation (piperidine)	13.51	323.1754	$C_{20}H_{22}N_2O_2$	-0.16	4.65 x 10^7
M24	Oxidation (ethyl of phenylpropanamide)	14.31	427.2380	$C_{28}H_{30}N_2O_2$	0.08	1.99 x 10^8
M25	*N*-Dealkylation (piperidine) + Oxidation (piperidine)	14.49	323.1755	$C_{20}H_{22}N_2O_2$	0.11	2.53 x 10^7
M26	Oxidation (ethyl of phenylpropanamide) + *N*-Oxidation (piperidine)	15.35	443.2332	$C_{28}H_{30}N_2O_3$	0.60	3.42 x 10^7
β'-phenylfentanyl (parent)		15.76	413.2588	$C_{28}H_{32}N_2O$	-0.19	2.44 x 10^8

2.2.1 Phase I reactions

2.2.1.1 N-Dealkylation

M17 was the metabolite with the most intense signal and eluted at 11.82 min with a base peak at *m/z* 309.1960, consistent with β'-phenylfentanyl *N*-dealkylation to β'-phenylfentanyl (−8C−8H) (Figure 3). The lack of parent fragments *m/z* 188.1434 and 281.2011, replaced by *m/z* 84.0807 and 177.1385, respectively, suggested the loss of the phenylethyl moiety. Fragment *m/z* 105.0698, also present in β'-phenylfentanyl MS^2 spectrum, was only produced by the phenethyl group of the phenylpropanamide moiety in M17. The metabolite was highly expected as *N*-dealkylation is common in fentanyl and other analogues [41,42]. M1 was produced by *N*-dealkylation at the amide group, forming 4-hydroxy-1-(2-phenylethyl)piperidine, as suggested by M1 base peak at *m/z* 206.1541 and fragments *m/z* 105.0698, 134.0963, 146.0962 and 188.1432, also detected in β'-phenylfentanyl MS^2 spectrum. The phenethylpiperidine moiety is common to most of FAs, and therefore this metabolites is not specific of β'-phenylfentanyl use.

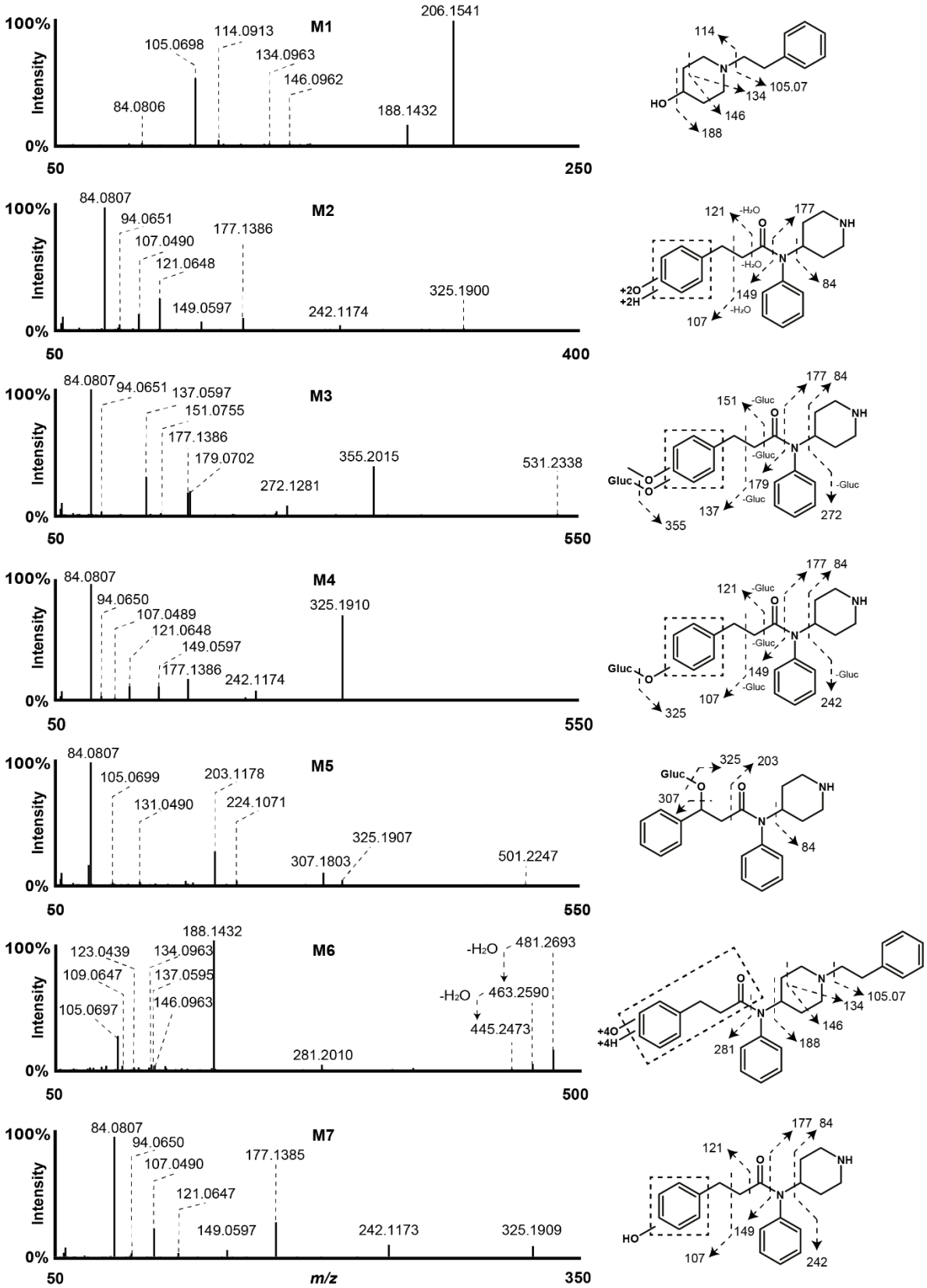

Figure 5. *β'-phenylfentanyl metabolites high-resolution tandem mass spectrometry spectra and suggested fragmentation in positive-ionization mode.*

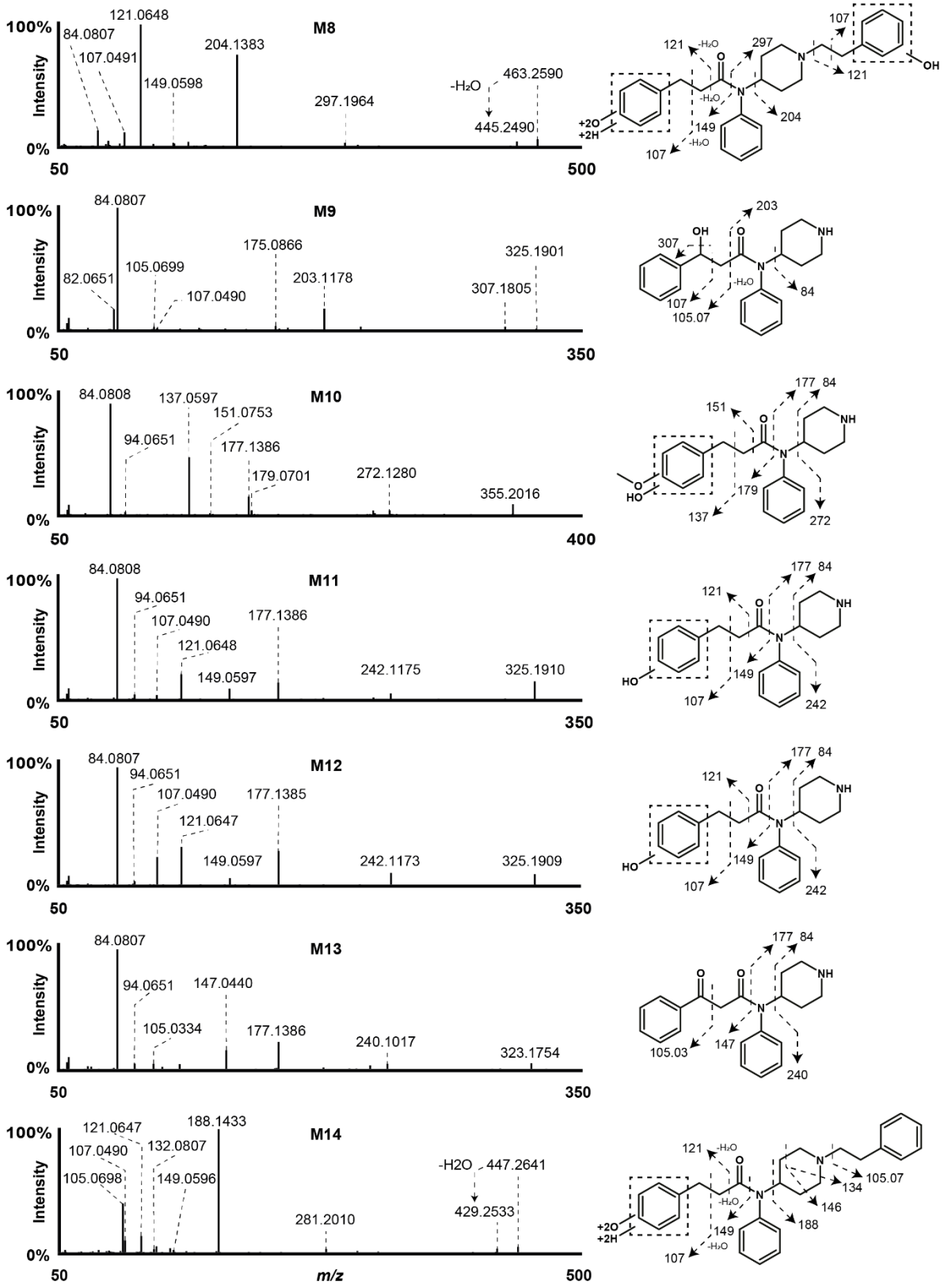

Figure 5. *(Continued)*

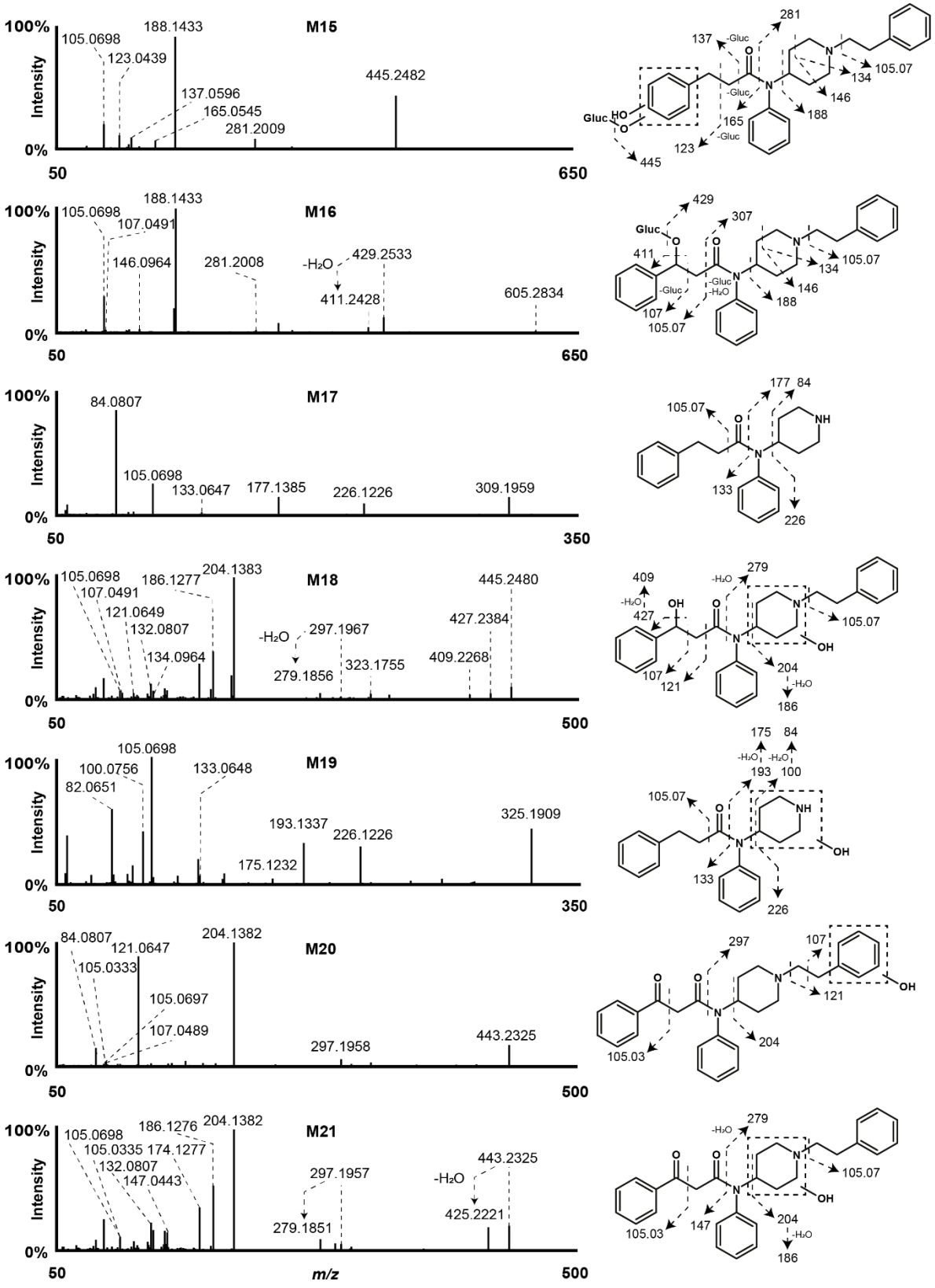

Figure 5. *(Continued)*

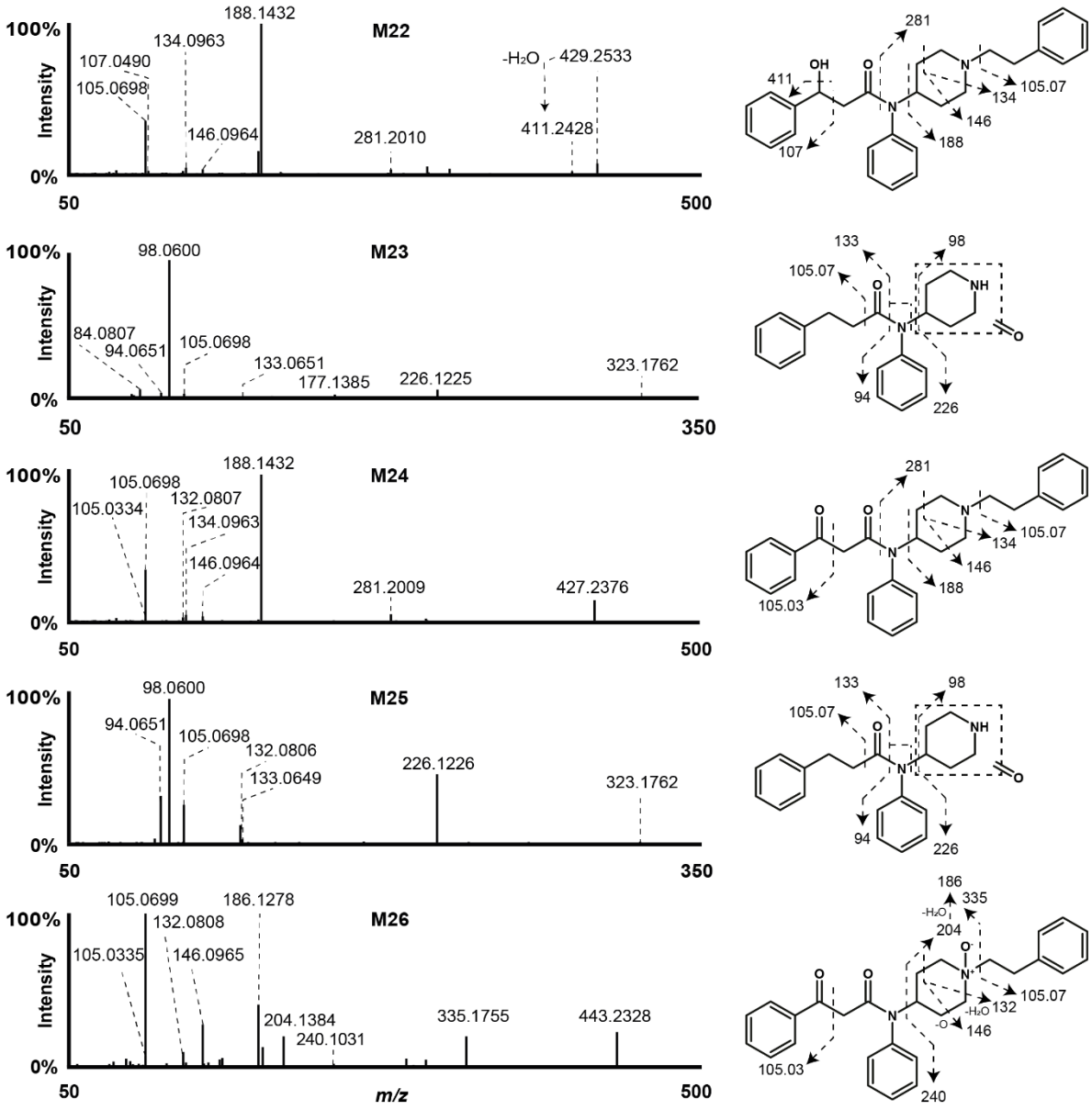

Figure 5. *(Continued)*

2.2.1.2 Hydroxylation

M22 eluted at 13.47 min and was the result of β'-phenylfentanyl hydroxylation (+O) as suggested by the +15.9949 Da mass shift from the parent and the water loss in M22 MS^2 spectrum. Fragments *m/z* 188.1432 and 281.2010, also present in β'-phenylfentanyl fragmentation, indicated that the transformation did not occur at the 4-ANPP moiety. Fragment *m/z* 107.0490 (hydroxytropylium ion) further indicated that the hydroxylation occurred at the phenylpropanamide moiety. Moreover, the water loss suggested that M22 was not hydroxylated at the phenyl ring, but rather at the C_{25} of the molecule. The hydroxylation induced the formation of an asymmetric carbon.

As no double peak was observed, it is not clear whether only one diastereoisomer was formed, or the two diastereoisomers were formed but co-eluted. Following the same reasoning, we found that M9 was generated through *N*-dealkylation (see section 2.2.1.1) and C_{25} hydroxylation. M7, M11, M12 and M19 also were formed by *N*-dealkylation (−8C−8H, and hydroxylation (+O), as suggested by the −88.0677 Da mass shift from β'-phenylfentanyl. As observed in M22 MS^2 spectrum, M7, M11 and M12 fragment *m/z* 107.0490 indicated the formation of a hydroxytropylium ion, suggesting a hydroxylation at the phenylpropanamide moiety. Fragments *m/z* 177.1386 and 84.0808 further indicated that the reaction occurred at the phenylpropanamide moiety. However, as opposed to M22, no water loss was detected, which may indicate that the reaction occurred at the phenyl group in the three metabolites (ortho, para and meta positions). In M19 MS^2 spectrum, fragments *m/z* 105.0698 and 133.0648 indicated that the phenylpropanamide group was intact. The lack of fragments *m/z* 84.0807 and 177.1385, replaced by *m/z* 100.0756 and 193.1337, respectively, and subsequent water losses, rather indicated that the hydroxylation occurred at the piperidine ring of the molecule. Following the same reasoning, M18 was a dihydroxylated metabolite of β'-phenylfentanyl, at C_{25} and the piperidine ring.

2.2.1.3 Oxidation

M24 eluted at 14.31 min with a base peak at *m/z* 427.2380, consistent with β'-phenylfentanyl oxidation (+O−2H). Parent fragments *m/z* 188.1432 and 281.2009 indicated that the reaction did not occur at the 4-ANPP moiety. Fragment *m/z* 105.0334,

however, indicated that the transformation occurred at the phenylpropanamide moiety, and more precisely at C_{25}. M24 LC-HRMS-MS peak was tailing up to a second minor peak at 18.18 min. This peak shape was consistent with a keto-enol tautomerism in favor of the keto form, and further confirmed the transformation. Similarly, M13 was produced by *N*-dealkylation and C_{25} oxidation; the keto and enol forms eluted at 10.18 and 13.98 min, respectively. Additionally, M20 and M21 were produced by C_{25} oxidation and hydroxylation at the phenyl of the phenethylpiperidine moiety (M20) or the piperidine ring (M21) (see section 2.2.1.3), while M26 was produced by C_{25} oxidation and *N*-oxidation at the piperidine ring, as suggested by the late retention time [33,43].

M23 and M25 also were formed by oxidation (+O−2H) after *N*-dealkylation (−8C−8H), and produced a base peak at *m/z* 323.1754. However, fragments *m/z* 226.1225 (*N*-phenyl-propanamide) and 98.0600 (oxo-piperidine) indicated that the oxidation occurred at M23 and M25 piperidine ring. Remarkably, M23 had the same mass as M13, although M23 signal was 50 times lower, and eluted along with M13 peak tail, between the two tautomeric forms. M23 MS^2 spectrum therefore contained M13 major fragments *m/z* 84.0807 and 177.1385, which made the structure elucidation challenging. M23 and M25 late elution, compared to that of M17, which was produced by *N*-dealkylation only, further pointed towards an oxidation at the piperidine ring [44–46]. The exact position of the carbonyl at the piperidine ring cannot be determined in present analytical conditions. The δ-lactam formation being favored [47], it may be hypothesized that M23 and M25 were oxidated at C_2 and C_3, respectively, M23 LC-HRMS-MS peak being more intense than that of M25.

2.2.1.4 Dihydrodiol formation

Benzenedihydrodiols are common metabolites of benzene in humans via epoxidation and subsequent epoxide hydration [48]. M14 is a dihydrodiol derivative (+2H+2O) of β'-phenylfentanyl, as suggested by the +34.0056 Da mass shift from the parent. M14 MS^2 spectrum contains β'-phenylfentanyl fragments *m/z* 105.0689, 188.1433 and 281.2010 which exclude any possible transformation at the 4-ANPP moiety. As observed with M22, fragment *m/z* 107.0490 was the hydroxytropylium ion, which was formed after water loss in M14 fragmentation, indicating that the transformation occurred at the phenyl ring of the phenylpropanamide moiety. Further M14 *N*-dealkylation led to M2, while further M14

hydroxylation at the phenyl ring of the phenethylpiperidine led to M8. Interestingly, the signals of M8 fragments *m/z* 107.0491 and 121.0648 are more intense compared to M14 MS^2 spectrum due to the phenol contribution. Benzenedihydrodiol derivatives may be potent carcinogens, and can be converted in vivo into less reactive catechols by the dihydrodiol dehydrogenase [49,50]. In the present experiments, catechols were not detected, although we identified their phase II derivative.

Further transformation of M14 led to the polyolic metabolite M6 (+4H+4O), characterized by multiple water losses. M6 may be formed by double dihydrodiol formation at the phenyl ring of the phenylpropanamide moiety. However, the accurate position of the hydroxyl groups cannot be determined in the present analytical conditions.

2.2.2 Phase II reactions

2.2.2.1 O-Glucuronidation

Glucuronidation occurred in five metabolites, as suggested by the glucuronide loss from precursors (−176.0315 Da). M5 and M16 were *O*-glucuronides derivatives from M9 and M22 respectively, while M4 was M7, M11 or M12 *O*-glucuronide.

2.2.2.2 O-Methylation

N-Dealkylation (−8C−8H), catechol formation, and subsequent *O*-methylation (+C+2H) occurred in M10, as suggested by the −58.0572 Da mass shift from β'-phenylfentanyl and fragments *m/z* 84.0808, 137.0597 and 177.1386 in M10 MS^2 spectrum. M3 was M10 *O*-glucuronide.

2.2.3 Comparison to phenylfentanyl metabolism

Phenylfentanyl (*N*-phenyl-*N*-[1-(2-phenylethyl)piperidin-4-yl]benzamide) is a β'-phenylfentanyl analogue with a phenylamide group instead of a phenylpropanamide. It was incubated with human hepatocytes along with β'-phenylfentanyl in the very same

conditions (same hepatocyte suspension, reagents, solvents, same concentration and incubation time), as previously reported [33]. Interestingly, although the structural difference between the two analogues is minor, their metabolic patterns differ substantially. Phenylfentanyl produced fewer metabolites than β'-phenylfentanyl: major metabolites included 4-ANPP, through amide hydrolysis, and further transformations (5 of 13 metabolites), which were not detected with β'-phenylfentanyl. However, although *N*-dealkylation to phenylnorfentanyl was also a major reaction, it produced only one subsequent minor metabolite, as opposed to β'-phenylfentanyl. The phenylpropanamide group is more susceptible to metabolic transformations, and the phenyl group is more accessible to metabolic enzymes in β'-phenylfentanyl phenylpropanamide group, explaining the discrepancies between the two analogues.

The metabolic fate of the major metabolites is suggested in Figure 4.

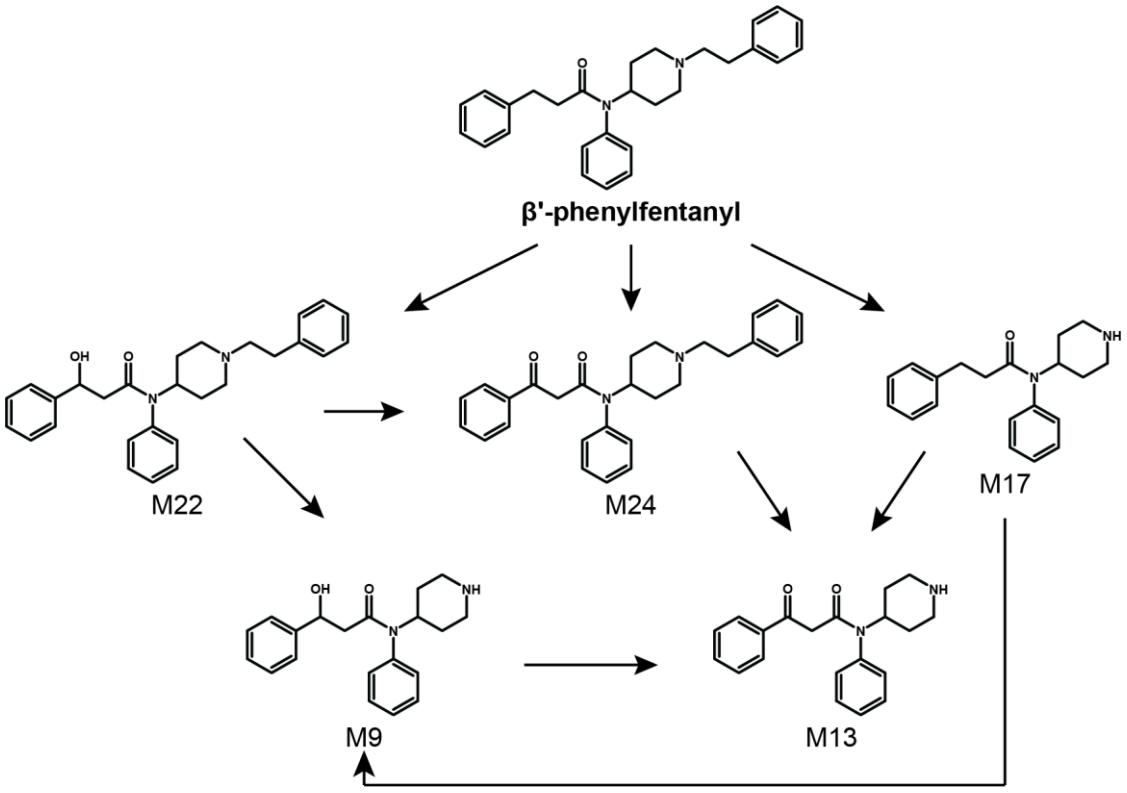

Figure 6. *β'-Phenylfentanyl suggested metabolic fate (only major metabolites).*

3. Human metabolism and basic pharmacokinetic evaluation of AP-238

3.1 Materials and Methods

3.1.1 Chemicals and reagents

Formic acid (Rotipuran® ≥98%, p.a.), sodium hydroxide (≥99%, p.a., pellets), and potassium hydrogen phosphate (≥99%, p.a.) were obtained from Carl Roth (Karlsruhe, Germany). ACN LC-MS grade and ammonium formate 10 M (99.995%) were bought from SigmaAldrich (Steinheim, Germany). Isopropanol (Prepsolv®) was obtained from Merck (Darmstadt, Germany). Acetic acid glacial (USP, EP, and JP grades) was purchased from VWR (Darmstadt, Germany). pHLMs (50 donors, 20 mg/mL protein in 250 mM sucrose), NADPH-regenerating Solutions A and B (reductase activity 0.43 µmol/min*mL), and potassium phosphate buffer 0.5 M (pH 7.5) were purchased from Corning (New York, USA). NADPH regenerating Solution A consisted of 26 mM $NADP^+$, 66 mM glucose-6-phosphate, and 66 mM $MgCl_2$ in water. NADPH-regenerating Solution B consisted of 40 U/mL glucose-6-phosphate dehydrogenase in 5 mM sodium citrate. Merck (Darmstadt, Germany) produced the β-glucuronidase/aryl-sulfatase (*Helix pomatia*) used for conjugate cleavage.

AP-238 HCl (purity ≥98%) was provided as hydrochloride from Cayman Chemical (Ann Arbor, MI, USA). Full analytical data (GC–MS, NMR, and FTIR) on the structural characterization of AP-238 have already been provided.[28] Deionized water was prepared using a Medica® Pro deionizer from ELGA (Celle, Germany). Blank urine samples were donated by a volunteer and tested for the absence of AP-238 metabolites prior to use. Mobile phase A (1% ACN, 0.1% HCOOH, and 2 mM $NH_4^+HCOO^-$ in water) and mobile phase B (0.1% HCOOH and 2 mM $NH_4^+HCOO^-$ in ACN) were freshly prepared prior to analysis. The sodium formate/acetate clusters solution, used for external and internal mass calibration of the QToF-MS instrument, was prepared by mixing 250 mL deionized water, 250 mL isopropanol, 750 µL acetic acid, 250 µL formic acid, and 500 µL sodium hydroxide 1 M.

3.1.2 pHLM incubation

In vitro phase I metabolites of AP-238 were tentatively generated applying a pHLM assay, which was performed by adding 0.5 µL of a 1 mg/mL reference standard solution (final concentration of 10 µg/mL in ACN) to 49.5 µL of a reaction mixture consisting of 2.5 µL pHLM, 2.5 µL NADPH-regenerating Solution A, 0.5 µL NADPH regenerating Solution B, 10 µL phosphate buffer 0.5 M (pH 7.4), and 34 µL deionized water. The reaction was performed during a 2 h-long incubation at 37 °C and was terminated by the addition of 150 µL ice-cold ACN. After addition of 25 µL of a 10 M ammonium formate solution, the sample was centrifuged for 4 min at 13,000 rpm. Then, the organic layer was transferred into a separate vial. For LC-QToF-MS analysis, 30 µL of the extracts was evaporated to dryness under a stream of nitrogen and reconstituted with 30 µL mobile phase A/B (95/5, v/v). Two blank pHLM samples, one containing no reference standard (zero-control) and the other one containing no pHLM-enzymes (blank-control), were processed accordingly and served as negative controls. The experiments were performed in triplicates.

3.1.3 Self-administration study

For investigation of the in vivo metabolism, a volunteer (Caucasian male, 29 years old, 72 kg body weight) ingested one gelatine capsule containing AP-238 (1.19 mg). The amount of the drug was extrapolated from previous pharmacological studies and after consulting self-assessment online fora to minimize the risk for adverse effects [32,51].One serum and one urine sample was taken before ingestion of the drug and four serum samples (30 min, 1 h, 2 h and 24 h post intake) as well as six urine samples (over four days) were taken. All samples were stored at –20 °C until analysis. Approval by an ethics committee is not required for self-experiments in Germany.

3.1.4 Sample preparation

For the investigation of the in vivo AP-238 phase I main metabolites, two urines and four whole blood samples from four forensic toxicological routine cases were analyzed. Sample preparation was conducted as previously described, with minor modifications [31].

After addition of 100 µL phosphate buffer (pH 6) and 10 µL β-glucuronidase/aryl-sulfatase to 100 µL of urine/blood, the samples were incubated at 45 °C (1 h). Afterwards, 1 mL ice-cold ACN and 100 µL of a 10 M ammonium formate solution were added. The mixture was shaken (overhead mixing) for 5 min, centrifuged for 10 min at 14,000 rpm (Heraeus Megafuge 1.0, Thermo Scientific, Schwerte, Germany). 1 mL of the organic layer was then transferred into a separate vial and evaporated to dryness under a stream of nitrogen. Finally, the samples were reconstituted in 50 µL mobile phase A/B (95/5, v/v) prior to LC-QToF-MS analysis. Negative control samples (blank urine) were prepared accordingly. Serum and urine samples collected after the controlled self-administration study were submitted to the same sample preparation procedure.

3.1.5 Identification of tentative main metabolites (LC-QToF-MS)

LC-QToF-MS analysis was performed on an Impact II QToF instrument coupled with an Elute RS HPLC system (Bruker Daltonik, Bremen, Germany). Chromatographic separation was performed on a Kinetex® C18 column (2.6 µm, 100 Å, 100, 2.1 mm; Phenomenex, Aschaffenburg, Germany) Gradient elution was 0 min, 5%B; 1 min, 5%B; 8 min, 15%B; 12 min, 30%B; 14 min, 65%B; 15 min, 95%B held for two minutes; 17.1-20 min gradual return to initial condition. The flow rate was set to 0.5 mL/min. Autosampler and column oven temperature were set to 10 °C and 40 °C, respectively. The injection volume was 5 µL. HyStar™ ver. 3.2 and DataAnalysis (DA) ver. 4.2 (Bruker Daltonik, Bremen, Germany) were used for data acquisition and processing, respectively.

The MS was operated in positive electrospray ionization (ESI^+) mode acquiring spectra in the *m/z* range of 50-650. The dry gas temperature was set to 200 °C with a dry gas flow of 8.0 L/min. The nebulizer gas pressure was 2 bar.

3.1.5.1 Untargeted data mining

Full scan and auto MS^2 data were acquired in one run at an acquisition rate of 4.0 Hz. In a second run, full scan and broadband collision-induced dissociation (bbCID) data were acquired to screen for additional metabolites and to prevent missing product ion spectra of minor metabolites during auto MS^2 scan. The resulting spectra were compared with a list of

hypothetical metabolites, based on the known biotransformation reactions of structurally similar NSOs [25,52]. The resulting hits for the molecular ions of anticipated metabolites were further analyzed with defined quadrupole mass selection (±0.5 Da) and retention time windows.

3.1.5.2 Targeted data mining

All identified molecular ions of the metabolites were added to a scheduled precursor ion list (SPL) and further characterized in MS^2 mode to produce product ion spectra.

Additionally, the maximum number of MS^2 cycles that were performed on a precursor ion was set to the value of three ('active exclusion'). If a precursor exceeded this number of cycles, the molecular ion was excluded from further analysis for 1.0 min. Using this workflow, pure product ion spectra of even low abundant metabolites can be obtained, even if they co-elute with highly abundant metabolites or highly abundant signals originating from the matrix. The collision energy applied for bbCID was 30 ± 6 eV. Full scan and MS^2 data were acquired at an acquisition rate of 2.0 Hz in one run. Nitrogen was used as collision gas. The voltages for the capillary and end plate offset were 2,500 and 500 V, respectively. External and internal mass calibration was performed using sodium formate/acetate clusters and high-precision calibration (HPC) mode.

3.1.5.3 Data post-processing

For comparison of the relative abundances of the metabolites for human samples and pHLM assays, peak area ratios were calculated by dividing pHLM (n=3 replicates), post-mortem urine (n=2 samples) and blood (n=4 samples) mean peak areas of each metabolite by the peak area of the most abundant metabolite in the respective matrix. The metabolite with the highest peak area was set to 100% and the relative abundances of all detected metabolites were ranked. The following criteria were applied for metabolite identification: mass error of the precursor ion <5 ppm, mass error of diagnostic product ions <10 ppm, signal-to-noise ratio >3:1 and matching isotope pattern.

3.1.6 Semi-quantitation for basic pharmacokinetics evaluation

Calibration range and limit of detection (LOD) (0.2 ng/mL)were determined by spiking blank serum and urine samples with AP-238 at concentrations from 0.5 to 100 ng/mL and fortified with 10 µl of internal standard (*O*-desmethyltramadol-D6 100 ng/ml). The LOD criteria were fulfilled for signal-to-noise ratios of at least 3:1 for the target and qualifier ion. To account for heteroscedasticity, a weighted calibration model (1/x) was applied. Since for the assessment of preliminary basic pharmacokinetic data semi-quantitative results were sufficient, a full method validation according to forensic guidelines was not carried out [53].

Analyses were performed on a Shimadzu Nexera X2 LC-30AD (Duisburg, Germany) coupled to QTRAP 5500 triple quadrupole linear ion trap instrument (Sciex, Darmstadt, Germany). The LC system was equipped with a Kinetex® F5 column (2.6 µm, 100 x 2.1 mm) (Phenomenex, Aschaffenburg, Germany) with a corresponding pre-column (2.1 mm) from Phenomenex. Autosampler temperature was maintained at 10 °C and the injection volume was 10 µL. Chromatrographic conditions were as follows (flow 0.5 mL/min): an initial hold at 5% B for 1 min, increased to 22.5% B at 4.5 min, then to 32.5 %B at 10.75 min, then to 95 %B at 13.5 min, holding at 95% B for 2 min and then decreasing to initial conditions in 0.5 min, held for 3.5 min. Total runtime was 19.5 min. Samples were analyzed in ESI positive mode with an ion spray voltage of 4,500 V. The gas settings were as follows: curtain gas 40 psi, collision gas medium, ion source gas (1) 60 psi, ion source gas (2) 70 psi. Source temperature was set to 500 °C.

3.2 Results and Discussion

3.2.1 AP-238 human metabolism

Eluting at 8.52 min at the previously reported LC-QToF-MS conditions, AP-238 ($[M + H]^+$ at *m/z* 287.2118) was detected in the pHLM blank-control. The same mass and retention time were found in the real samples. AP-238 fragmentation pattern was consistent with the scientific literature and displayed characteristic fragments at *m/z* 91.0542, 117.0699 and 169.1335 corresponding to the tropylium, cinnamyl and acylpiperazine moiety (Figure 7) [27,30].

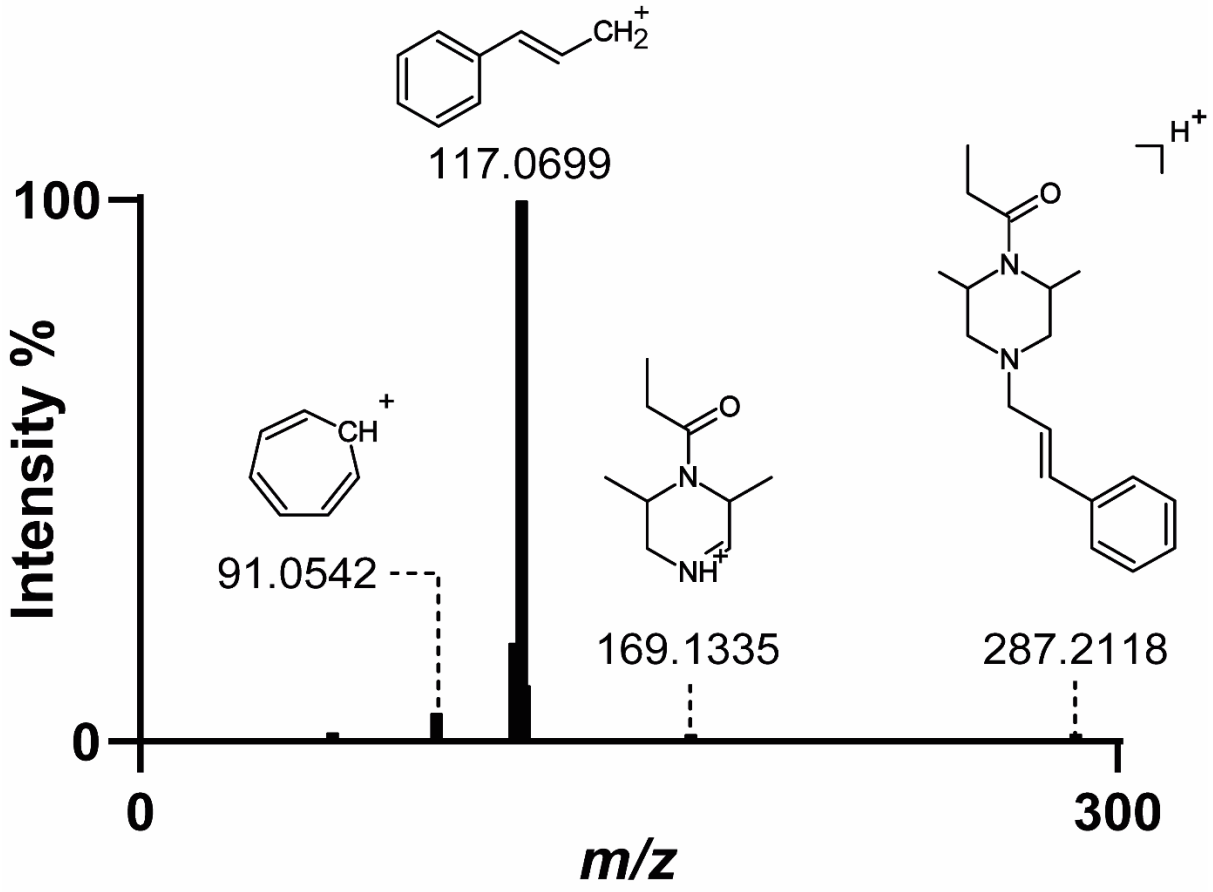

Figure 7. *AP-238 LC-qToF-MS spectrum and suggested fragmentation in positive-ionization mode.*

After enzymatic cleavage of glucuronides and sulphates, the analysis of the human phase I metabolism led to the detection of 32 metabolites in urine and 26 in blood, assigned to the following biotransformations: mono and dihydroxylation, *N*-deacylation, dihydrodiol formation, oxidation and combination thereof that were listed from M1 to M32 by ascending

retention time (Figure 8-10; Table 3). All 12 metabolites anticipated in vitro using the pHLM assay, as well as all 26 metabolites detected in blood were confirmed in authentic urine samples. Although the initial purpose of this study was to elucidate the AP-238 phase I metabolic pathway, five additional phase II metabolites, obtained via *O*-methylation, were also reported. In Figure 11, the fragmentation pattern of AP-238 main metabolites, as shown in both authentic urine and blood samples, is displayed. It should be mentioned that identification of glucuronide or sulphate metabolites was not an aim of this study.

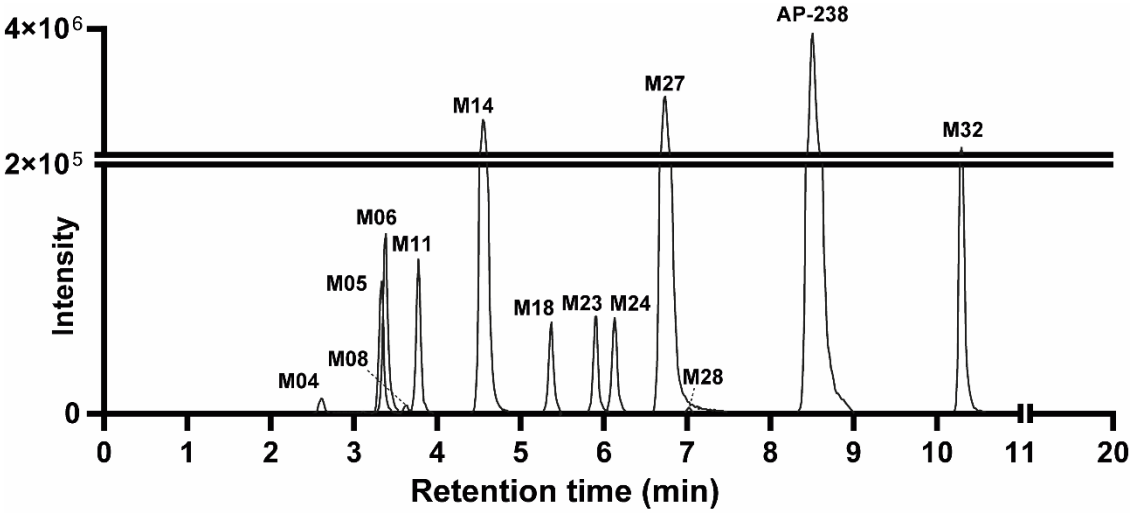

Figure 8. *Extracted-ion chromatogram of AP-238 and metabolites in positive-ionization mode obtained after 2 h incubation with pooled human liver microsomes. Mass tolerance, 5 ppm.*

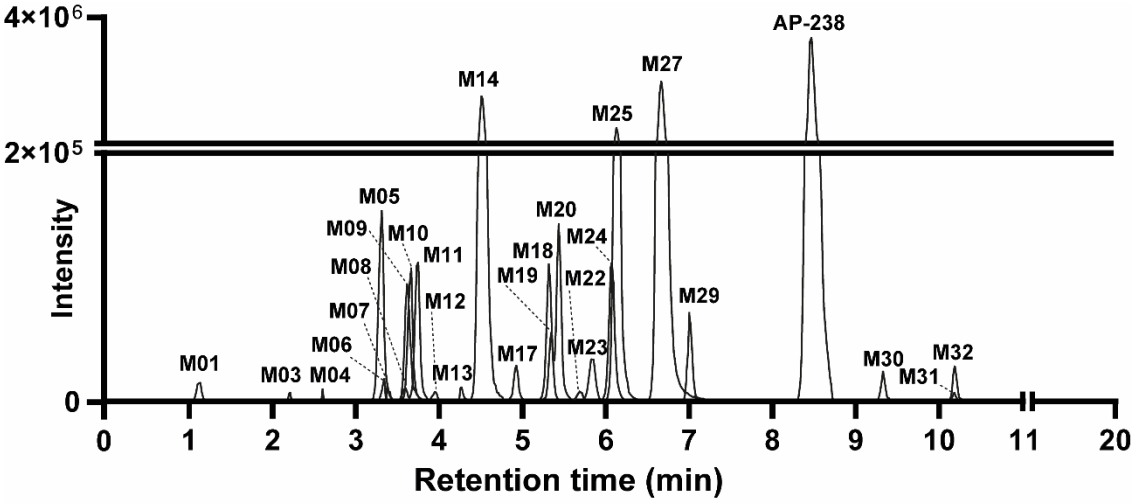

Figure 9. *Extracted-ion chromatogram of AP-238 and metabolites in positive-ionization mode obtained from post-mortem whole blood (sample n°3). Mass tolerance, 5 ppm.*

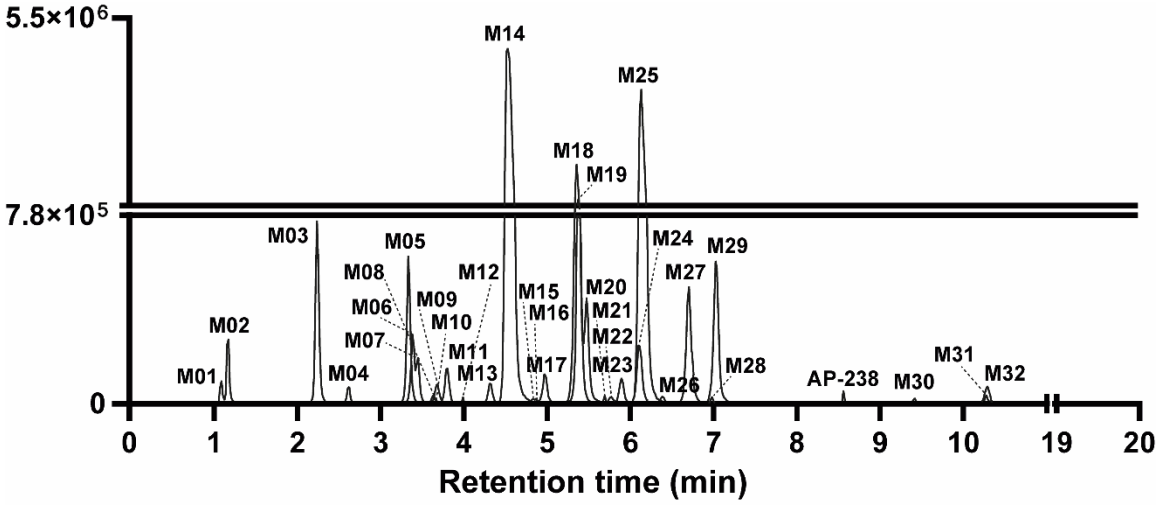

Figure 10. *Extracted-ion chromatogram of AP-238 and metabolites in positive-ionization mode obtained from post-mortem urine (sample n°2). Mass tolerance, 5 ppm.*

Table 3. *Identified in vitro and in vivo phase I metabolites of AP-238 (M00) in the order of their retention time (RT). For ranking the metabolites, relative mean area ratios (MAR) of each metabolite calculated by comparison to the most abundant metabolite (100% in bold).*

ID	RT (min)	Biotransformation	Calculated $[M + H]^+$	Formula $[M + H]^+$	Mass error (ppm)	Diagnostic product ions (m/z)	Diagnostic product ions formula	Diagnostic product ions mass error (ppm)	Post-mortem urine ranking position (MAR %)	Post-mortem blood ranking position (MAR %)	pHLM ranking position (MAR %)
M00	8.52	-	287.2118	$C_{18}H_{27}N_2O$	0.7	117.0699 169.1335	C_9H_9 $C_9H_{17}N_2O$	-0.9 -0.2	-	-	-
M01	1.17	Hydroxylation (C) + N-deacylation	247.1805	$C_{15}H_{23}N_2O$	0.2	115.123 133.0648	$C_6H_{15}N_2$ C_9H_9O	-0.5 -0.9	9 (7.39%)	11 (3.85%)	-
M02	1.57	Hydroxylation (C) + N-deacylation	247.1805	$C_{15}H_{23}N_2O$	0.3	115.123 133.0648	$C_6H_{15}N_2$ C_9H_9O	0.4 0.1	31 (0.25%)	-	-
M03	2.25	DiOH (C and A)	319.2016	$C_{18}H_{27}N_2O_3$	-0.7	115.123 133.0648	$C_6H_{15}N_2$ C_9H_9O	-0.4 -0.6	8 (10.1%)	17 (1.4%)	-
M04	2.63	DiOH (C and A)	319.2016	$C_{18}H_{27}N_2O_3$	0.4	115.123 133.0648	$C_6H_{15}N_2$ C_9H_9O	-0.3 -0.5	17 (1.55%)	23 (0.4%)	10 (0.47%)
M05	3.33	DiOH (C and P) + N-deacylation	263.1754	$C_{15}H_{23}N_2O_2$	0.3	131.1179 133.0648	$C_6H_{15}N_2O$ C_9H_9O	-0.8 -0.6	4 (17.22%)	4 (7.9%)	7 (3.37%)
M06	3.40	DiOH (C)	319.2016	$C_{18}H_{27}N_2O_3$	1	149.0597 171.1492	$C_9H_9O_2$ $C_9H_{19}N_2O$	0 0.8	11 (6.24%)	21 (0.99%)	5 (5.36%)
M07	3.44	DiOH (C and P)	319.2016	$C_{18}H_{27}N_2O_3$	0.5	133.0648 187.1441	C_9H_9O $C_9H_{19}N_2O_2$	0.2 0.5	12 (4.71%)	20 (0.91%)	-
M08	3.64	Dihydrodiol	321.2173	$C_{18}H_{29}N_2O_3$	1.8	183.1492 265.1911	$C_{15}H_{25}N_2O_2$ $C_9H_{19}N_2O_2$	1.7 -1.3	30 (0.26%)	23 (0.4%)	12 (0.15%)
M09	3.67	N-deacylation	231.1856	$C_{15}H_{23}N_2$	0.6	91.0542 117.0699	C_7H_7 C_9H_9	1 0.6	22 (0.77%)	9 (4.92%)	-
M10	3.71	Hydroxylation (C)	303.2067	$C_{18}H_{27}N_2O_2$	-0.2	133.0648 171.1492	C_9H_9O $C_9H_{19}N_2O$	0.9 1	18 (1.41%)	6 (5.84%)	-
M11	3.81	Dihydrodiol	321.2173	$C_{18}H_{29}N_2O_3$	1.1	183.1492 265.1911	$C_{15}H_{25}N_2O_2$ $C_9H_{19}N_2O_2$	2.8 0.9	19 (1.37%)	10 (4.13%)	4 (5.77%)
M12	3.99	DiOH (C) + O-methylation	333.2173	$C_{19}H_{29}N_2O_3$	2.8	163.0754 171.1492	$C_{10}H_{11}O_2$ $C_9H_{19}N_2O$	1 -0.2	25 (0.65%)	22 (0.52%)	-
M13	4.36	DiOH (C)	319.2016	$C_{18}H_{27}N_2O_3$	1.4	149.0597 171.1492	$C_9H_9O_2$ $C_9H_{19}N_2O$	1.2 1.9	20 (1.04%)	24 (0.29%)	-

M14	4.53	Hydroxylation (C)	303.2067	$C_{18}H_{27}N_2O_2$	1.9	133.0648 171.1492	C_9H_9O $C_9H_{19}N_2O$	1 1.7	**1 (100%)**	2 (70.86%)	2 (67.79%)
M15	4.74	DiOH (C and P)	319.2016	$C_{18}H_{27}N_2O_3$	2	133.0648 187.1441	C_9H_9O $C_9H_{19}N_2O_2$	0.9 0.8	28 (0.41%)	-	-
M16	4.87	DiOH (C and P)	319.2016	$C_{18}H_{27}N_2O_3$	1.2	133.0648 187.1441	C_9H_9O $C_9H_{19}N_2O_2$	-0.2 -0.5	29 (0.29%)	-	-
M17	4.98	Hydroxylation (C)	303.2067	$C_{18}H_{27}N_2O_2$	2.6	133.0648 171.1492	C_9H_9O $C_9H_{19}N_2O$	2 1.8	15 (3.14%)	18 (1.05%)	
M18	5.36	Hydroxylation (P)	303.2067	$C_{18}H_{27}N_2O_2$	0.2	117.0699 185.1285	C_9H_9 $C_9H_{17}N_2O_2$	-0.6 -0.7	6 (14.4%)	7 (5.18%)	8 (3.35%)
M19	5.38	DiOH (C) + O-methylation	333.2173	$C_{19}H_{29}N_2O_3$	1.9	163.0754 171.1492	$C_{10}H_{11}O_2$ $C_9H_{19}N_2O$	-0.2 -0.3	7 (13.69%)	14 (2.94%)	-
M20	5.48	Hydroxylation (C)	303.2067	$C_{18}H_{27}N_2O_2$	1.4	133.0648 171.1492	C_9H_9O $C_9H_{19}N_2O$	0.6 0.8	13 (3.93%)	13 (3.18%)	-
M21	5.70	DiOH (C) + O-methylation	333.2173	$C_{19}H_{29}N_2O_3$	0	163.0754 171.1492	$C_{10}H_{11}O_2$ $C_9H_{19}N_2O$	1.9 1.3	23 (072%)	-	-
M22	5.73	DiOH (C and P) + N-deacylation	263.1754	$C_{15}H_{23}N_2O_2$	0.7	131.1179 133.0648	$C_6H_{15}N_2O$ C_9H_9O	0.3 0.4	21 (0.9%)	25 (0.11%)	-
M23	5.89	Oxydation + N-deacylation	245.1648	$C_{15}H_{23}N_2O_2$	-0.8	113.1073 133.0648	$C_6H_{13}N_2$ C_9H_9O	-0.6 -0.3	10 (7.09%)	15 (2.83%)	9 (2.49%)
M24	6.10	Hydroxylation (P)	303.2067	$C_{18}H_{27}N_2O_2$	1.4	117.0699 185.1285	C_9H_9 $C_9H_{17}N_2O_2$	1.3 2	16 (2.68%)	8 (5.15%)	6 (3.92%)
M25	6.14	DiOH (C) + O-methylation	333.2173	$C_{19}H_{29}N_2O_3$	1.3	163.0754 171.1492	$C_{10}H_{11}O_2$ $C_9H_{19}N_2O$	0.5 -0.7	2 (84.45%)	3 (39.38%)	-
M26	6.39	Hydroxylation (C)	303.2067	$C_{18}H_{27}N_2O_2$	0.7	133.0648 171.1492	C_9H_9O $C_9H_{19}N_2O$	0.7 1.4	24 (0.7%)	-	-
M27	6.67	Hydroxylation (P) + N-deacylation	247.1805	$C_{15}H_{23}N_2O$	0.2	114.0913 117.0699	$C_6H_{13}N_2O$ C_9H_9O	0.4 -0.5	5 (14.96%)	**1 (100%)**	**1 (100%)**
M28	7.02	DiOH (C and P)	319.2016	$C_{18}H_{27}N_2O_3$	1.7	133.0648 187.1441	C_9H_9O $C_9H_{19}N_2O_2$	0.7 0.9	27 (0.41%)	-	11 (0.16%)
M29	7.03	Hydroxylation (P)	303.2067	$C_{18}H_{27}N_2O_2$	1.4	117.0699 185.1285	C_9H_9 $C_9H_{17}N_2O_2$	0.9 -1.2	3 (32.6%)	5 (7.36%)	-
M30	9.35	O-methylation	317.2224	$C_{19}H_{29}N_2O_2$	2.6	107.048 147.0804	C_7H_7 $C_{10}H_{10}O$	1.1 0.2	32 (0.16%)	16 (1.53)	-

M31	10.22	Hydroxylation (P) + N-deacylation	247.1805	$C_{15}H_{23}N_2O$	0.7	114.0913 117.0699	$C_6H_{13}N_2O$ C_9H_9O	1.9 0.2	26 (0.51%)	19 (1.04%)	-
M32	10.38	Hydroxylation (P)	303.2067	$C_{18}H_{27}N_2O_2$	2.8	117.0699 185.1285	C_9H_9 $C_9H_{17}N_2O_2$	1.7 3.4	14 (3.74%)	12 (3.48%)	3 (19.48%)

Footnotes

A: Acyl moiety; C: Cinnamyl moiety; DiOH: Dihydroxylation; P: Piperazin moiety; pHLM: Pooled human liver microsomes

3.2.2 Phase I reactions

3.2.2.1 Hydroxylation(s)

M14 was the metabolite with the most intense signal in all authentic urines and the second among the detected blood metabolites. Given its protonated mass at *m/z* 303.2067, M14 was the result of AP-238 hydroxylation (+O), as indicated by the + 15.9949 Da mass shift from the parent. The fragment at *m/z* 133.0648 suggests that the biotransformation occurred at the cinnamyl moiety. M10, M17 and M26 shared the same fragmentation pattern, while slight differences of intensity were observed for fragments at *m/z* 115.123 and at *m/z* 171.1492, piperazine and acylpiperazine moieties respectively, in the spectrum of M20. Interestingly, the fragment at *m/z* 105.0699, characteristic of a phenethyl cation, occurred in all above-mentioned metabolites' spectra, preventing the determination of the exact location of hydroxylation within the cinnamyl moiety. It is well-known that phenyl allyl cations can easily undergo intramolecular cyclization to the corresponding indanyl cations, with possible migration of functional groups [54] Thus, the fragment at *m/z* 105.0699 could be generated after fragmentation of the indanyl cycle. However, under the present analytical conditions, the exact location of the hydroxylation in M10, M14, M17, M20 and M26 cannot be determined.

The hydroxylation at the AP moiety represented another frequent biotransformation pathway of AP-238, leading to the formation of the positional isomers M18, M24, M29 and M32. The detection of specific ion fragments at *m/z* 185.1285 and at *m/z* 117.0699 and the absence of *m/z* 115.123 suggest the localization of the hydroxyl at the piperazine core. Once again, it is not possible to determine the exact site of hydroxylation, although the late elution of M29 and M32 may indicate the presence of *N*-oxides.[14,33,55] Taking into consideration the mean area ratios (MAR%), M29 was the third most abundant metabolite in urine and the fifth in blood.

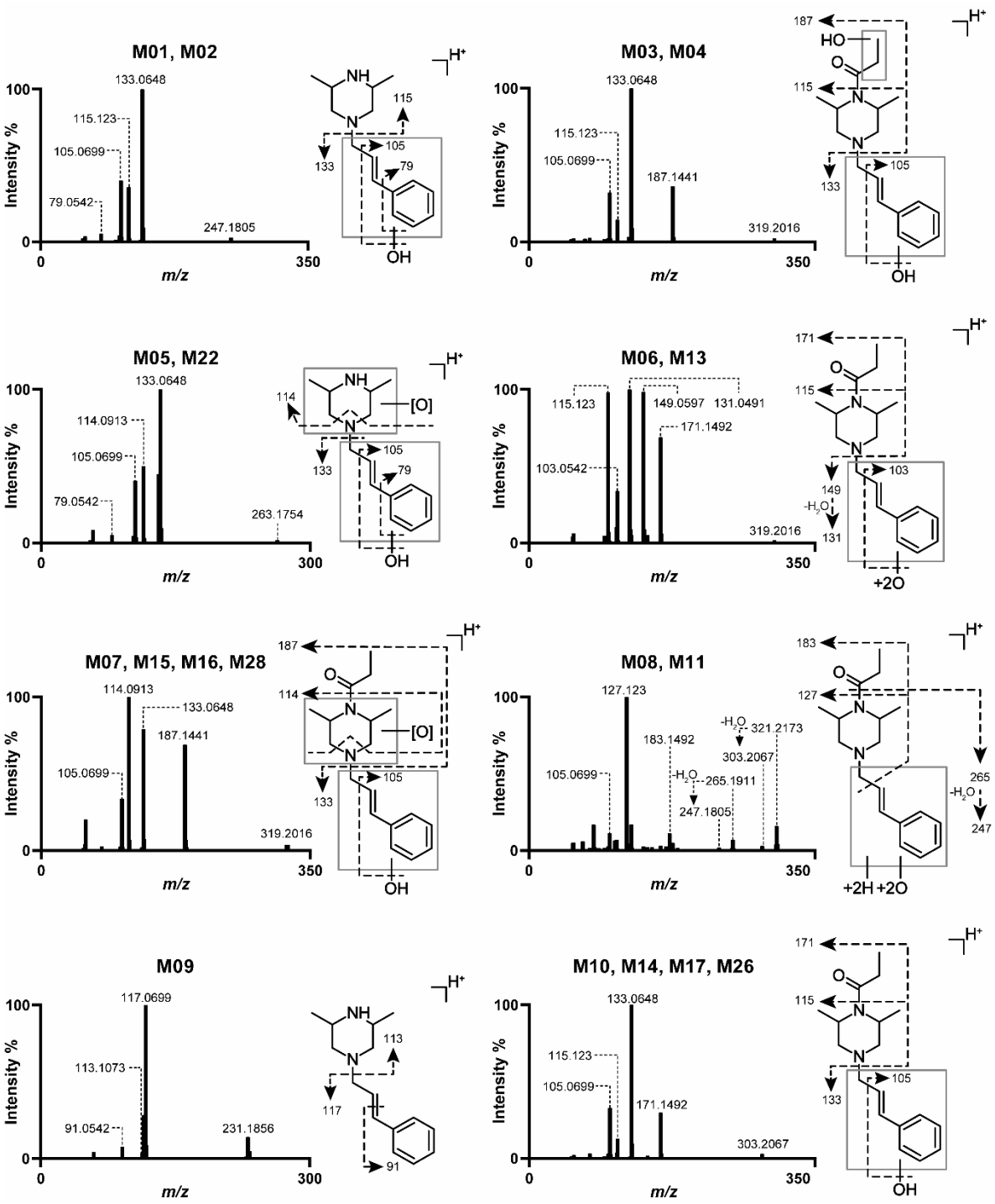

Figure 11. *AP-238 metabolites LC-qToF-MS spectra and suggested fragmentation in positive-ionization mode.*

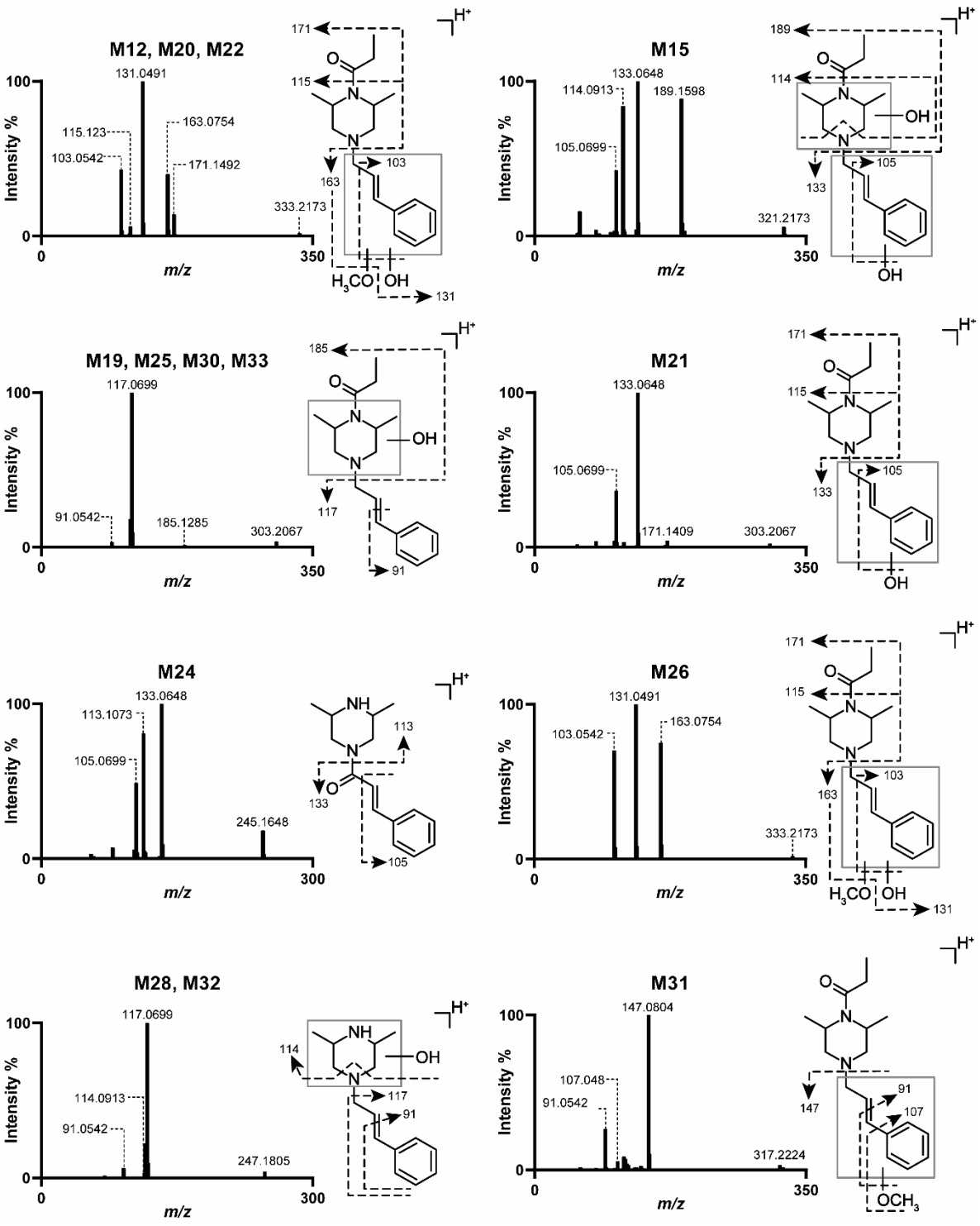

Figure 11. *(Continued)*

Eight dihydroxylated metabolites ($[M + H]^+$ at *m/z* 319.2016) were identified, characterized by a mass shift of 31.9898 Da (+2O) from the parent. The most dominant was M03, which was, together with M04, hydroxylated once at the cinnamyl moiety and once at the acylic portion as suggested by the fragments at *m/z* 185.1285, *m/z* 115.123 and *m/z* 133.0648. The presence of the fragment at *m/z* 114.0913, characteristic of the hydroxylated 2,6-dimethylpiperazine cleavage, instead of that at *m/z* 115.123, allowed the identification of M07, M15, M16 and M28 as dihydroxylated metabolites at the cinnamyl moiety and at the piperazine core. M06 and M13 can be interpreted as dihydroxylation of AP-238's at the cinnamyl moiety as indicated by the fragments at *m/z* 149.0597.

3.2.2.2 N-Deacylation

M09 ($[M + H]^+$ at *m/z* 231.1856) emerged from the *N*-deacylation of the piperazine, as suggested by the –56.0262 Da mass shift from the parent. Its MS^2 spectrum was similar to that of AP-238, except for the characteristic fragment at *m/z* 169.1335. Following the same reasoning, there is a good chance that M01 and M02 originate from the metabolites bearing a hydroxyl at the cinnamyl moiety. M27 and M31, as well, can be interpreted as the *N*-deacyl *N*-oxides generated from M29 and M32, as suggested by their late elution. Similarly, M07, M15, M16 and M28 would plausibly be intermediates for the formation of their *N*-deacyl analogues M05 and M22.

3.2.2.3 Dihydrodiol formation

Benzenedihydrodiols are common metabolites of benzene-bearing substances and are formed via epoxidation and subsequent epoxide hydratation.[32]. M08 and M11 ($[M + H]^+$ at *m/z* 321.2173) are AP-238 dihydrodiol derivatives as suggested by the +34.0056 Da mass shift from the parent. The water loss observed in their MS^2 spectra is extremely favored to reestablish the aromaticity of the ring. However, the cleavage between the α and the β carbon of the allyl moiety, which generates the fragments at *m/z* 183.1492 and at *m/z* 127.123, may indicate the presence of a proximal heteroatom. If the dihydrodiol formation involved the allylic double bond, it would be possible that M08 and M11 were the pair of diastereomers originated after the formation of two asymmetric centers. Once again, unfortunately, it is

impossible to determine the exact position of the two hydroxyl groups.

3.2.2.4 Reduction and Oxidation

Finally, M23 was a minor metabolite generated after oxidation of the hydroxyl group bound to the C1 of the phenyl allyl substituent. It is possible that M23 stems from an intermediate hydroxylated metabolite originating from M09 or after oxidation of M01 and M02.

3.2.3 Phase II reactions

3.2.3.1 O-Methylation

M12, M19, M21 and M25 ($[M + H]^+$ at *m/z* 333.2173) were generated after dihydroxylation and methylation of one of the hydroxyl groups of the cinnamyl moiety, as indicated by the fragment at *m/z* 163.0754. The loss of the methoxy group led then to the formation of the ion at *m/z* 131.0491. Remarkably, the most abundant metabolite (M25) was characterized by a lower intensity of ions at *m/z* 115.123 and at *m/z* 171.1492 when compared to M12, M19 and M21. This suggests a difference in the location of these two substituents, although their exact position cannot be determined from our data. In humans, the methylation of aromatic hydroxy groups is catalyzed by two different enzymes: catechol *O*-methyltransferase (COMT) and phenol *O*-methyltransferase (PMT). Mechanistically, a transfer of the methyl moiety from the co-factor *S*-adenosyl-methionine onto one of the aromatic hydroxyl groups was postulated.[56] Since COMTs are responsible for the metabolism of catecholamines, it is likely that at least one of the metabolites M06 and M13 bears a catechol moiety, acting as an intermediate in the formation of M12, M19, M21 or M25. On the other hand, PMT could have also been responsible for the methylation of phenolic groups of one or both of the above mentioned cinnamyl-dihydroxylated metabolites, although this represents a minor metabolic pathway. Another possible way is represented by the hydroxylation of M30, the methoxy metabolite of AP-238. This minor metabolite might be originated from one of the cinnamyl-hydroxylated metabolites ($[M + H]^+$ at *m/z* 303.2067) under the action of PMT, as indicated by the fragment at *m/z* 149.0804. Since PMT substrates

are phenols, the methoxy group is suggested to be located at the benzene ring, as further confirmed by the ion at *m/z* 107.0491.

Due to the absence of *S*-adenosyl-methionine as co-factor, all the metabolites in this section were not predicted by the pHLM assay. The metabolic fate of AP-238 is reported in Figure 12.

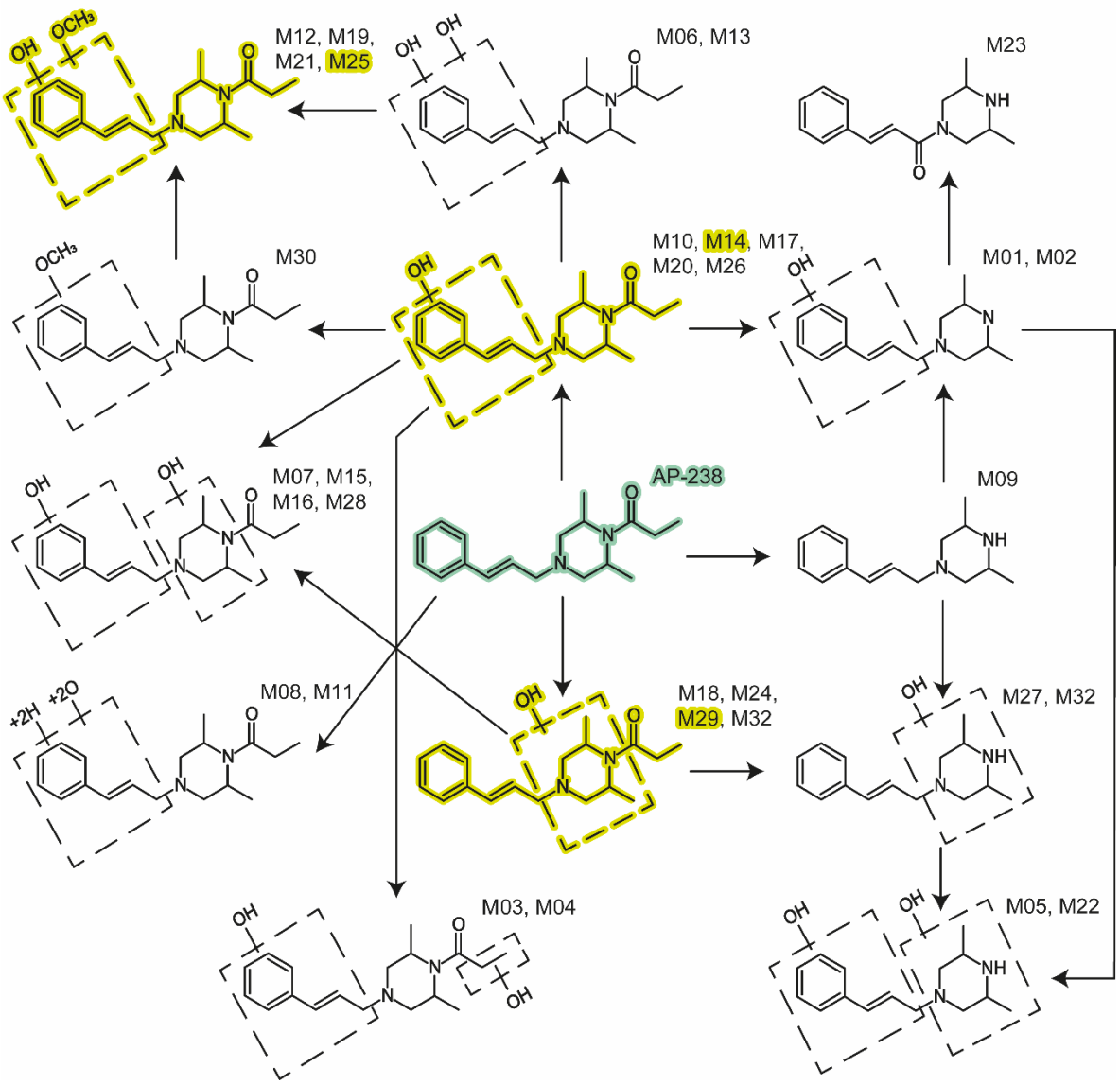

Figure 12. *Postulated in vivo biotransformation pathways of AP-238 as investigated in authentic urine samples. AP-238 and most abundant metabolites are highlighted in green and yellow respectively.*

3.2.4 Basic pharmacokinetic data and evaluation of metabolites for death cases and abstinence control

After oral uptake, the peak concentration in serum of AP-238 was reached after 30 min (2.87 ng/mL), gradually decreasing 1 h (2.57 ng/mL) and 2 h (1.63 ng/mL) post-ingestion, displaying a relatively rapid gastrointestinal absorption, in line with the studies of Carrano et al. for AP-237 [22,23]. Twenty-four hours post-intake, the AP-238 serum concentration was below the range of calibration (≈ 0.05 ng/mL, cf. Figure 13). The volunteer did not experience any physical or mental impairment during the study. Considering the relatively low dose ingested, this was not surprising.

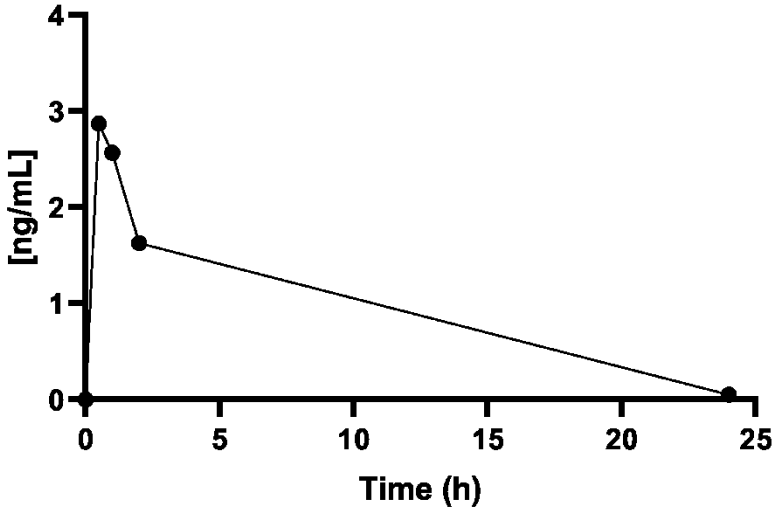

Figure 13. *Serum concentrations over time received by LC-MS/MS analysis of samples obtained after a single oral administration of 1.19 mg AP-238 HCl to a human volunteer.*

To prove the uptake of illicit drugs, urine is often the preferred biological matrix for forensic and clinical toxicology, particularly in drug abstinence testing when longer detection windows are needed [57]. For this purpose, six urine samples obtained after the self-administration of AP-238 were submitted to qualitative analysis using LC-QToF-MS. Inclusion criteria listed in section 3.1.5 were applied and peak areas were normalized for the creatinine values (Figure 14). Only traces of unmetabolized AP-238 were detected in urine, starting from the sample obtained 50 min up to the sample collected 21 h and 20 min post-ingestion. Metabolites M14, M25, M27 and M29 could be detected in the urine samples obtained between 50 min and 94 h post-ingestion. For abstinence control, the monitoring of these four specific metabolites in urine is recommended.

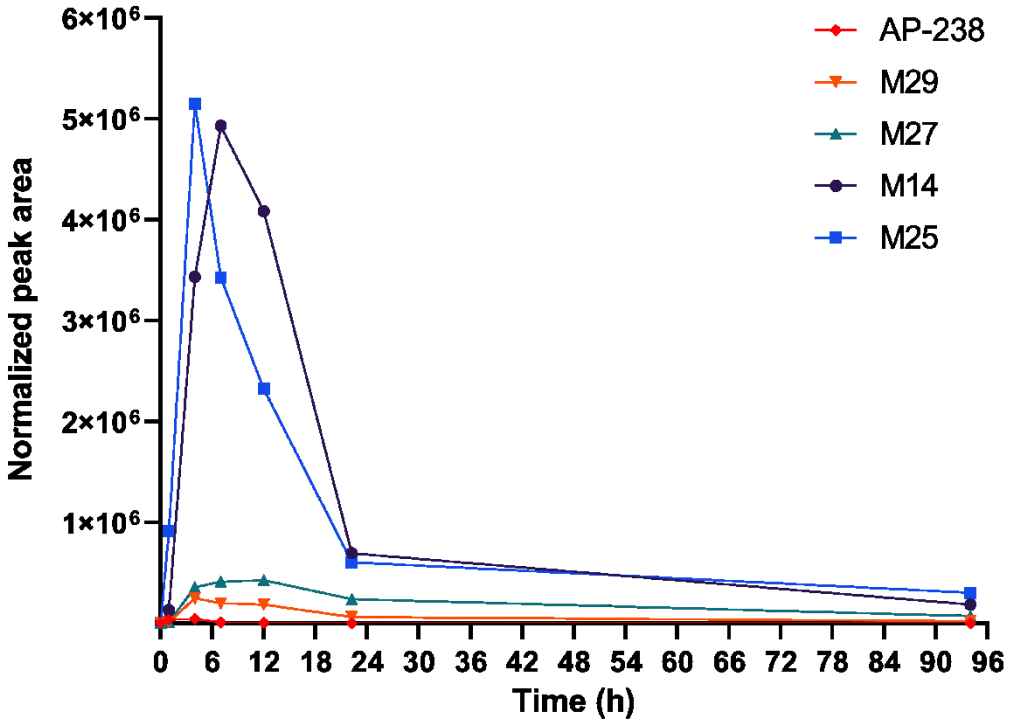

Figure 14. *Peak areas for the main metabolites M14, M25, M27 and M29 received by LC-qToF-MS analysis after conjugate cleavage of samples obtained after a single oral administration of 1.19 mg AP-238 HCl to a human volunteer. All values were normalized to a creatinine concentration of 100 mg/dL.*

Remarkably, although it was assigned the rank #2 in the post-mortem urine metabolism study (Table 3), M25 was the most dominant metabolite for the first 3 hours after being temporarily displaced by M14 (rank #1 in Table 3) that reached a maximum 5 h 40 min post-ingestion. This might be a starting point for estimation of the time that passed between consumption and death in post-mortem cases, although it has to be mentioned that dose, route of administration and other variables would have to be considered for valid interpretation. It has to be kept in mind that NSOs are mainly consumed by injecting, smoking or through nasal insufflation, and not by oral administration.[58] Parenteral intake could thus result in stronger effects at the same dose and different kinetic profiles.

4. Coclusions

The occurrence of NSOs, and particularly FAs and APs opioids, is of rising concern. Developing analytical methods for the detection of their metabolites is extremely important to correctly assign the cause of intoxication in clinical or forensic cases and to complement analytical strategies for abstinence control.

4.1 β'-phenylfentanyl in vitro metabolism

For the first time, the β'-phenylfentanyl metabolic profile was characterized using cryopreserved primary human hepatocytes LC-HRMS-MS analysis and software-assisted data mining. 26 different metabolites produced by phase I and phase II transformations, mostly through *N*-dealkylation, oxidation, hydroxylation, *O*-glucuronidation, *O*-methylation and combinations thereof, were identified. β'-phenylfentanyl (M17, N-phenyl-N-4-piperidinyl-benzenepropanamide) and further metabolites M13 (1-oxo-N-phenyl-N-4-piperidinyl-benzenepropanamide) and M9 (1-hydroxy-N-phenyl-N-4-piperidinyl-benzenepropanamide) are suggested as the main biomarkers of β'-phenylfentanyl consumption, and the inclusion of its fragmentation pattern in online libraries mzCloud and HighResNPS has been proposed.

β'-phenylfentanyl metabolism substantially differed from that of phenylfentanyl, a close structural analogue, in the same incubation conditions. Together, these results show that predicting NPS metabolism is challenging, and highlight the importance of experimental data. The in vitro model hence reported provides preliminary results on β'-phenylfentanyl human metabolism, which should be confirmed with samples from authentic positive cases.

4.2 AP-238 human metabolism and basic pharmacokinetic evaluation

The in vitro and in vivo metabolism of AP-238 was investigated using a pHLM assay, samples of death cases and samples from a controlled oral self-administration experiment, resulting in the detection of a total of 32 metabolites.

Several isomeric metabolites with the same MS^2 spectra but different retention times were detected after biotransformation of AP-238. To clearly identify the location of the functional groups introduced by metabolic reactions, the synthesis of reference material or

the isolation of the metabolites of interest for structure elucidation, e.g. by NMR spectroscopy, would be required. Thus, in the present study, it was not possible to elucidate the exact chemical structures of the majority of the metabolites.

As a second limitation, the in vivo MAR% were based on the chromatographic peak areas and might not accurately reflect absolute concentrations, given possible differences in ionization efficiency and matrix effects. Matrix effects were also not evaluated for the semi-quantitative determination of AP-238 in serum.

Thirdly, additional phase II metabolites could be found in authentic samples when omitting the enzymatic cleavage step with β-glucuronidase/arylsulfatase or when assays based on hepatocytes, pHLS9 or animal models are performed. However, as routine analysis usually involves a hydrolysis step, phase I metabolites are preferred, and the vast portfolio of specific biomarkers identified is more than sufficient to prove the uptake of AP-238.

Among the detected metabolites, particularly M14, M25, M27 and M29 can be recommended to be monitored in abstinence screening due to their relatively high abundance.

5. References

1. Grafinger, K.E.; Liechti, M.E.; Liakoni, E. Clinical Value of Analytical Testing in Patients Presenting with New Psychoactive Substances Intoxication. *Br. J. Clin. Pharmacol.* **2020**, *86*, 429–436, doi:10.1111/bcp.14115.

2. Tabarra, I.; Soares, S.; Rosado, T.; Gonçalves, J.; Luís, Â.; Malaca, S.; Barroso, M.; Keller, T.; Restolho, J.; Gallardo, E. Novel Synthetic Opioids - Toxicological Aspects and Analysis. *Forensic Sci. Res.* **2019**, *4*, 111–140, doi:10.1080/20961790.2019.1588933.

3. Solimini, R.; Pichini, S.; Pacifici, R.; Busardò, F.P.; Giorgetti, R. Pharmacotoxicology of Non-Fentanyl Derived New Synthetic Opioids. *Front. Pharmacol.* **2018**, *9*, 654, doi:10.3389/fphar.2018.00654.

4. Giorgetti, A.; Brunetti, P.; Pelotti, S.; Auwärter, V. Detection of AP-237 and Synthetic Cannabinoids on an Infused Letter Sent to a German Prisoner. *Drug Test. Anal.* **2022**, *14*, 1779–1784, doi:10.1002/dta.3351.

5. Armenian, P.; Vo, K.T.; Barr-Walker, J.; Lynch, K.L. Fentanyl, Fentanyl Analogs and Novel Synthetic Opioids: A Comprehensive Review. *Neuropharmacology* **2018**, *134*, 121–132, doi:10.1016/j.neuropharm.2017.10.016.

6. Brunetti, P.; Giorgetti, R.; Tagliabracci, A.; Huestis, M.A.; Busardò, F.P. Designer Benzodiazepines: A Review of Toxicology and Public Health Risks. *Pharm. Basel Switz.* **2021**, *14*, 560, doi:10.3390/ph14060560.

7. EMCDDA. European Drug Report: Trends and Developments. 2022 Available online: https://www.emcdda.europa.eu/system/files/publications/14644/TDAT22001ENN.pdf.

8. Peacock, A.; Bruno, R.; Gisev, N.; Degenhardt, L.; Hall, W.; Sedefov, R.; White, J.; Thomas, K.V.; Farrell, M.; Griffiths, P. New Psychoactive Substances: Challenges for Drug Surveillance, Control, and Public Health Responses. *Lancet Lond. Engl.* **2019**, *394*, 1668–1684, doi:10.1016/S0140-6736(19)32231-7.

9. Brunetti, P.; Pirani, F.; Carlier, J.; Giorgetti, R.; Busardò, F.P.; Lo Faro, A.F. A 2017-2019 Update on Acute Intoxications and Fatalities from Illicit Fentanyl and Analogs. *J. Anal. Toxicol.* **2021**, *45*, 537–554, doi:10.1093/jat/bkaa115.

10. Giorgetti, A.; Brunetti, P.; Pelotti, S.; Auwärter, V. Detection of AP-237 and Synthetic Cannabinoids on an Infused Letter Sent to a German Prisoner. *Drug Test. Anal.* **2022**, *14*, 1779–1784, doi:10.1002/dta.3351.

11. EMCCDA. Spotlight On… Fentanils and Other New Opioids. Available online: https://www.emcdda.europa.eu/spotlights/fentanils-and-other-new-opioids_en (accessed on 24 August 2022).

12. Lamy, F.R.; Daniulaityte, R.; Barratt, M.J.; Lokala, U.; Sheth, A.; Carlson, R.G. "Etazene, Safer than Heroin and Fentanyl": Non-Fentanyl Novel Synthetic Opioid Listings on One Darknet Market. *Drug Alcohol Depend.* **2021**, *225*, 108790, doi:10.1016/j.drugalcdep.2021.108790.

13. Vandeputte, M.M.; Cannaert, A.; Stove, C.P. In Vitro Functional Characterization of a Panel of Non-Fentanyl Opioid New Psychoactive Substances. *Arch. Toxicol.* **2020**, *94*, 3819–3830, doi:10.1007/s00204-020-02855-7.

14. Grafinger, K.E.; Wilde, M.; Otte, L.; Auwärter, V. Pharmacological and Metabolic Characterization of the Novel Synthetic Opioid Brorphine and Its Detection in Routine Casework. *Forensic Sci. Int.* **2021**, *327*, 110989, doi:10.1016/j.forsciint.2021.110989.

15. EMCDDA. European Drug Report 2022: Trends and Developments. Available online: https://www.emcdda.europa.eu/system/files/publications/14644/TDAT22001ENN.pdf (accessed on 24 August 2022).

16. Pardo, B.; Taylor, J.; Caulkins, J.; Reuter, P.; Kilmer, B. The Dawn of a New Synthetic Opioid Era: The Need for Innovative Interventions. *Addict. Abingdon Engl.* **2021**, *116*, 1304–1312, doi:10.1111/add.15222.

17. Clinton, H.A.; Thangada, S.; Gill, J.R.; Mirizzi, A.; Logan, S.B. Improvements in Toxicology Testing to Identify Fentanyl Analogs and Other Novel Synthetic Opioids in Fatal Drug Overdoses, Connecticut, January 2016–June 2019. *Public Health Rep.* **2021**, *136*, 80S-86S, doi:10.1177/00333549211042829.

18. UNODC. World Drug Rreport 2021. Booklet 3 Available online: https://www.unodc.org/unodc/en/data-and-analysis/wdr-2021_booklet-3.html (accessed on 22 April 2022).

19. Di Trana, A.; Pichini, S.; Pacifici, R.; Giorgetti, R.; Busardò, F.P. Synthetic Benzimidazole Opioids: The Emerging Health Challenge for European Drug Users. *Front. Psychiatry* **2022**, *13*, 858234, doi:10.3389/fpsyt.2022.858234.

20. EMCDDA. EMCDDA–Europol 2017 Annual Report on the Implementation of Council Decision 2005/387/JHA Available online: https://www.emcdda.europa.eu/system/files/publications/9282/20183924_TDAN18001ENN_PDF.pdf.

21. UNODC. New Psychoactive Substances Portal and International Collaborative Exercise Portal Available online: https://www.unodc.org/LSS/Home/BothAreas (accessed on 22 February 2023).

22. Carrano, R.A.; Kimura, K.K.; Landes, R.C.; McCurdy, D.H. General Pharmacology of a New Analgesic-AP-237. *Arch. Int. Pharmacodyn. Ther.* **1975**, *213*, 28–40.

23. Carrano, R.A.; Kimura, K.K.; McCurdy, D.H. Analgesic and Tolerance Studies with AP-237, a New Analgesic. *Arch. Int. Pharmacodyn. Ther.* **1975**, *213*, 41–57.

24. Irikura, T.; Masuzawa, K.; Nishino, K.; Kitagawa, M.; Uchida, H.; Ichinoseki, N.; Ito, M. New Analgetic Agents. V. 1-Butyryl-4-Cinnamylpiperazine Hydrochloride and Related Compounds. *J. Med. Chem.* **1968**, *11*, 801–804, doi:10.1021/jm00310a022.

25. Resnik, K.; Brandão, P.; Alves, E.A. DARK Classics in Chemical Neuroscience: Bucinnazine. *ACS Chem. Neurosci.* **2021**, *12*, 3527–3534, doi:10.1021/acschemneuro.1c00522.

26. Zhang, C.; Han, S.-Q.-G.-W.; Zhao, H.; Lin, S.; Hasi, W.-L.-J. Detection and Quantification of Bucinnazine Hydrochloride Injection Based on SERS Technology. *Anal. Sci. Int. J. Jpn. Soc. Anal. Chem.* **2018**, *34*, 1249–1255, doi:10.2116/analsci.18P158.

27. CFSRE. AP-238 Monograph. Available online: https://www.npsdiscovery.org/wp-content/uploads/2020/11/AP-238_111120_CFSRE-Toxicology_Report.pdf (accessed on 25 August 2022).

28. EMCCDA. EDND Available online: https://ednd2.emcdda.europa.eu/ednd/substanceProfiles/1010 (accessed on 22 April 2022).

29. Cignarella, G.; Testa, E. 2,6-Dialkylpiperazines. IV. 1-Propionyl-4-Substituted Cis-2,6-Dimethylpiperazines Structurally Related to the Analgetic 8-Acyl-3,8-Diazabicyclo[3.2.1]Octanes. *J. Med. Chem.* **1968**, *11*, 592–594, doi:10.1021/jm00309a039.

30. Fogarty, M.F.; Vandeputte, M.M.; Krotulski, A.J.; Papsun, D.; Walton, S.E.; Stove, C.P.; Logan, B.K. Toxicological and Pharmacological Characterization of Novel Cinnamylpiperazine Synthetic Opioids in Humans and in Vitro Including 2-Methyl AP-237 and AP-238. *Arch. Toxicol.* **2022**, doi:10.1007/s00204-022-03257-7.

31. Giorgetti, A.; Brunetti, P.; Haschimi, B.; Busardò, F.P.; Pelotti, S.; Auwärter, V. Human Phase-I Metabolism and Prevalence of Two Synthetic Cannabinoids Bearing an Ethyl Ester Moiety: 5F-EDMB-PICA and EDMB-PINACA. *Drug Test. Anal.* **2022**, doi:10.1002/dta.3405.

32. Brunetti, P.; Lo Faro, A.F.; Di Trana, A.; Montana, A.; Basile, G.; Carlier, J.; Busardò, F.P. β'-Phenylfentanyl Metabolism in Primary Human Hepatocyte Incubations: Identification of Potential Biomarkers of Exposure in Clinical and Forensic Toxicology. *J. Anal. Toxicol.* **2023**, *46*, e207–e217, doi:10.1093/jat/bkac065.

33. Di Trana, A.; Brunetti, P.; Giorgetti, R.; Marinelli, E.; Zaami, S.; Busardò, F.P.; Carlier, J. In Silico Prediction, LC-HRMS/MS Analysis, and Targeted/Untargeted Data-Mining Workflow for the Profiling of Phenylfentanyl in Vitro Metabolites. *Talanta* **2021**, *235*, 122740, doi:10.1016/j.talanta.2021.122740.

34. de Bruyn Kops, C.; Šícho, M.; Mazzolari, A.; Kirchmair, J. GLORYx: Prediction of the Metabolites Resulting from Phase 1 and Phase 2 Biotransformations of Xenobiotics. *Chem. Res. Toxicol.* **2021**, *34*, 286–299, doi:10.1021/acs.chemrestox.0c00224.

35. Stork, C.; Embruch, G.; Šícho, M.; de Bruyn Kops, C.; Chen, Y.; Svozil, D.; Kirchmair, J. NERDD: A Web Portal Providing Access to in Silico Tools for Drug Discovery. *Bioinforma. Oxf. Engl.* **2020**, *36*, 1291–1292, doi:10.1093/bioinformatics/btz695.

36. Keller, B.O.; Sui, J.; Young, A.B.; Whittal, R.M. Interferences and Contaminants Encountered in Modern Mass Spectrometry. *Anal. Chim. Acta* **2008**, *627*, 71–81, doi:10.1016/j.aca.2008.04.043.

37. Wilde, M.; Pichini, S.; Pacifici, R.; Tagliabracci, A.; Busardò, F.P.; Auwärter, V.; Solimini, R. Metabolic Pathways and Potencies of New Fentanyl Analogs. *Front. Pharmacol.* **2019**, *10*, 238, doi:10.3389/fphar.2019.00238.

38. MzCloud – Advanced Mass Spectral Database Available online: https://www.mzcloud.org/ (accessed on 24 February 2023).

39. ChemSpider | Search and Share Chemistry Available online: http://www.chemspider.com/ (accessed on 24 February 2023).

40. Mardal, M.; Andreasen, M.F.; Mollerup, C.B.; Stockham, P.; Telving, R.; Thomaidis, N.S.; Diamanti, K.S.; Linnet, K.; Dalsgaard, P.W. HighResNPS.Com: An Online Crowd-Sourced HR-MS Database for Suspect and Non-Targeted Screening of New Psychoactive Substances. *J. Anal. Toxicol.* **2019**, *43*, 520–527, doi:10.1093/jat/bkz030.

41. Kanamori, T.; Togawa Iwata, Y.; Segawa, H.; Yamamuro, T.; Kuwayama, K.; Tsujikawa, K.; Inoue, H. Metabolism of Fentanyl and Acetylfentanyl in Human-Induced Pluripotent Stem Cell-Derived Hepatocytes. *Biol. Pharm. Bull.* **2018**, *41*, 106–114, doi:10.1248/bpb.b17-00709.

42. Gampfer, T.M.; Wagmann, L.; Park, Y.M.; Cannaert, A.; Herrmann, J.; Fischmann, S.; Westphal, F.; Müller, R.; Stove, C.P.; Meyer, M.R. Toxicokinetics and Toxicodynamics of the Fentanyl Homologs Cyclopropanoyl-1-Benzyl-4′-Fluoro-4-Anilinopiperidine and Furanoyl-1-Benzyl-4-Anilinopiperidine. *Arch. Toxicol.* **2020**, *94*, 2009–2025, doi:10.1007/s00204-020-02726-1.

43. Åstrand, A.; Töreskog, A.; Watanabe, S.; Kronstrand, R.; Gréen, H.; Vikingsson, S. Correlations between Metabolism and Structural Elements of the Alicyclic Fentanyl Analogs Cyclopropyl Fentanyl, Cyclobutyl Fentanyl, Cyclopentyl Fentanyl, Cyclohexyl Fentanyl and 2,2,3,3-Tetramethylcyclopropyl Fentanyl Studied by Human Hepatocytes and LC-QTOF-MS. *Arch. Toxicol.* **2019**, *93*, 95–106, doi:10.1007/s00204-018-2330-9.

44. Carlier, J.; Berardinelli, D.; Montanari, E.; Sirignano, A.; Di Trana, A.; Busardò, F.P. 3F-α-Pyrrolydinovalerophenone (3F-α-PVP) in Vitro Human Metabolism: Multiple in Silico Predictions to Assist in LC-HRMS/MS Analysis and Targeted/Untargeted Data Mining. *J. Chromatogr. B Analyt. Technol. Biomed. Life. Sci.* **2022**, *1193*, 123162, doi:10.1016/j.jchromb.2022.123162.

45. Swortwood, M.J.; Carlier, J.; Ellefsen, K.N.; Wohlfarth, A.; Diao, X.; Concheiro-Guisan, M.; Kronstrand, R.; Huestis, M.A. In Vitro, in Vivo and in Silico Metabolic Profiling of α-Pyrrolidinopentiothiophenone, a Novel Thiophene Stimulant. *Bioanalysis* **2016**, *8*, 65–82, doi:10.4155/bio.15.237.

46. Carlier, J.; Diao, X.; Giorgetti, R.; Busardò, F.P.; Huestis, M.A. Pyrrolidinyl Synthetic Cathinones α-PHP and 4F-α-PVP Metabolite Profiling Using Human Hepatocyte Incubations. *Int. J. Mol. Sci.* **2020**, *22*, 230, doi:10.3390/ijms22010230.

47. Vickers, S.; Polsky, S.L. The Biotransformation of Nitrogen Containing Xenobiotics to Lactams. *Curr. Drug Metab.* **2000**, *1*, 357–389, doi:10.2174/1389200003338929.

48. Snyder, R.; Hedli, C.C. An Overview of Benzene Metabolism. *Environ. Health Perspect.* **1996**, *104 Suppl 6*, 1165–1171, doi:10.1289/ehp.961041165.

49. Bolton, J.L.; Dunlap, T. Formation and Biological Targets of Quinones: Cytotoxic versus Cytoprotective Effects. *Chem. Res. Toxicol.* **2017**, *30*, 13–37, doi:10.1021/acs.chemrestox.6b00256.

50. Smithgall, T.E.; Harvey, R.G.; Penning, T.M. Regio- and Stereospecificity of Homogeneous 3 Alpha-Hydroxysteroid-Dihydrodiol Dehydrogenase for Trans-Dihydrodiol Metabolites of Polycyclic Aromatic Hydrocarbons. *J. Biol. Chem.* **1986**, *261*, 6184–6191.

51. De Baerdemaeker, K.S.C.; Dines, A.M.; Hudson, S.; Sund, L.J.; Waters, M.L.; Hunter, L.J.; Blundell, M.S.; Archer, J.R.H.; Wood, D.M.; Dargan, P.I. Isotonitazene, a Novel Psychoactive Substance Opioid, Detected in Two Cases Following a Local Surge in Opioid Overdoses. *QJM Mon. J. Assoc. Physicians* **2023**, *116*, 115–119, doi:10.1093/qjmed/hcac039.

52. Hassanien, S.H.; Layle, N.K.; Holt, M.C.; Zhao, T.; Iula, D.M. Cayman NPS Metabolism Monograph Available online: https://cdn2.caymanchem.com/cdn/cms/caymanchem/LiteratureCMS/2-methyl%20AP-237%20Metabolomics%20Monograph.pdf.

53. Huppertz, L.M.; Moosmann, B.; Auwärter, V. Flubromazolam - Basic Pharmacokinetic Evaluation of a Highly Potent Designer Benzodiazepine. *Drug Test. Anal.* **2018**, *10*, 206–211, doi:10.1002/dta.2203.

54. Olah, G.A.; Asensio, G.; Mayr, H. 1-Phenylallyl Cations and Their Rearrangement to Indanyl Cations in Superacidic Media. *J. Org. Chem.* **1978**, *43*, 1518–1520, doi:10.1021/jo00402a006.

55. Watanabe, S.; Vikingsson, S.; Roman, M.; Green, H.; Kronstrand, R.; Wohlfarth, A. In Vitro and In Vivo Metabolite Identification Studies for the New Synthetic Opioids Acetylfentanyl,

Acrylfentanyl, Furanylfentanyl, and 4-Fluoro-Isobutyrylfentanyl. *AAPS J.* **2017**, *19*, 1102–1122, doi:10.1208/s12248-017-0070-z.

56. Weinshilboum, R. Pharmacogenetics of Methylation: Relationship to Drug Metabolism. *Clin. Biochem.* **1988**, *21*, 201–210, doi:10.1016/s0009-9120(88)80002-x.

57. Concheiro, M.; Chesser, R.; Pardi, J.; Cooper, G. Postmortem Toxicology of New Synthetic Opioids. *Front. Pharmacol.* **2018**, *9*, 1210, doi:10.3389/fphar.2018.01210.

58. Pérez-Mañá, C.; Papaseit, E.; Fonseca, F.; Farré, A.; Torrens, M.; Farré, M. Drug Interactions With New Synthetic Opioids. *Front. Pharmacol.* **2018**, *9*, 1145, doi:10.3389/fphar.2018.01145.